, K. & Benney, D. The propagation of nonlinear shear flow with a free surface, *Studies in Applied* 76, 69–92.

erical simulation of the kinetic equations for sur- *Izv. Akad. Nauk SSSR. Fiz. Atmosf. Ok.*, 1990, **26**, lish translation: *Izvestia, Atmospheric and Oceanic* no.2, 118–123)

waves on shear currents: Solution of the boundary- *Fluid Mech.*, 1993, **253**, 565–584.

formation of a narrow angular spectrum of wind- nonlinear interaction between wind and waves, *Izv. Fiz. Atmosf. Ok.*, 1989, **25**, no.4, 411–420 (English *Atmospheric and Oceanic Physics*, 1989, **25**, no.4,

ear and Nonlinear Waves, Wiley, New York, 1974,

bility of periodic waves of finite amplitude on the id, *J. Appl. Math. Techn. Phys.*, 1968, **9**, 190–194.

nilga, A.V. On the dynamics of water wave spectra proximation, *Zh. Eksp. Teor. Fiz.*, 1981, **81**, 1318– ation: *Sov. Phys. JETP*, 1981, **54**, 700–706).

ira, V.I. 1990: On the formation of the directional s. *Zh. Eksp. Teor. Fiz.*, 1990, **98**, no.6(12), 1941– ion: *Sov. Phys. JETP*, 1990, **71**, no.6, 1091–1100).

akov, S.V., Novikov, S.P. & Pitaevsky, L.P. *Soli- thod of inverse scattering*, Nauka, Moscow, 1980, slation: Plenum Press, N.Y., 1984, 288 pp.)

slavsky, M.M. Generation and dissipation ranges on of weak turbulence theory for wind waves, *Izv. er. Fiz. Atmosf. Ok.*, 1983, **18**, no.10, 1066–1076 *Izvestia, Atmospheric and Oceanic Physics*, 1983,

le long-wave cut-off in the wind driven wave *Nauk SSSR Ser. Fiz. Atmosf. Ok.*, 1989, **25**, sh translation: *Izvestia, Atmospheric and Oceanic* –882).

Chapter 7

Direct modeling of one-dimensional nonlinear potential waves

D. Chalikov[a] & D. Sheinin[b]

[a]*UCAR/Ocean Modeling Branch/NCEP, 5200 Auth Road, Camp Spring, MD 20746, USA*

[b]*Massachussets Institute of Technology, Bldg E40-259, 1 Amherst St., Cambridge, MA 02139, USA*

Abstract

A method for numerical investigation of nonlinear wave dynamics based on direct hydrodynamical modeling of 1-D potential periodic surface waves is presented. By a nonstationary conformal mapping, the principal equations are rewritten in a surface-following coordinate system and reduced to two simple evolutionary equations for the elevation and the velocity potential of the surface. For stationary equations, the proposed approach coincides with the conventional complex variable method. For this case, numerical algorithms for solution of gravity (Stokes) and gravity-capillary wave equations are proposed, and examples of numerical solutions are given. The results imply that gravity-capillary waves do not approach Stokes waves as the capillarity coefficient decreases. Both stationary and nonstationary schemes use Fourier series representation for spatial approximation and the Fourier transform method to calculate nonlinearities. The nonstationary model was validated by simulation of propagating waves with initial conditions obtained as numerical (for gravity and gravity-capillary waves) or analytical (for pure capillary, or Crapper's waves) solutions of the stationary problem. The simulated progressive waves did not change their shape during long-term time integration, which indicates high accuracy of the scheme. Another criterion used for model validation was conservation of integral invariants of simulated multi-mode wave fields. A number of long-term model simulations of gravity, gravity-capillary, and pure capillary waves, with various initial conditions, were performed; for the simulated wave fields, distributions of energy and phase speed over fill spectra were analyzed. It was found that the wavenumber–frequency spectra are

[1]OMB contribution no. 131.

l separated into patterns lying along regularly located curves, with most of the rgy concentrated along the curves corresponding to free and bound waves. This of curves can be described by the equation $D(\omega/n, k/n) = 0 \quad (n = 1, 2, 3, ...)$, ere $D(\omega, k) = 0$ is approximated by the linear dispersion relation but does not ıcide with it, especially for large k where there is a tendency for the indicated ation to approximate a straight line. Some other properties of simulated wave ds were also analyzed; these included temporal evolution of the spectra and spatial ribution of the energy of perturbations. The method developed may be applied to road range of problems where the assumption of one-dimensionality is acceptable.

Introduction

mputational techniques for numerical solution of the Navier–Stokes ıations have brought new developments to geophysical fluid dynam- Using modern numerical models, the long-term evolution of several nplicated dynamical phenomena in different fluids, including the at- sphere, can be successfully simulated. However, the long-term simu- ion of a nonlinear multi-mode wave field is difficult to perform, since st numerical schemes for the Euler equations fail to provide sufficient uracy for treating nonlinearities in wave motion. The main source of or is primarily due to the finite difference representation of the vertical ucture of the flow when waves with different wavenumbers are present. us, theoretical and numerical investigations of surface gravity waves usually based on the equations for potential flow with a free surface. this case the flow is fully determined by the form of the surface and the ocity potential on the surface and in its vicinity. The potential mo- n assumption, of course, idealizes the phenomenon, since actual wave tion is both rotational and turbulent. Fortunately, potential theory es many results which agree well with observations. For example, it is l-known that even linear theory yields phase velocity estimates with accuracy of the order of 1%. A much more sophisticated theory, deal- with nonlinear wave–wave interactions (Hasselmann, 1962), which is ɔ based on the potential motion assumption, gives results which are ıfirmed by experimental data.

The main advantage of the potential motion approximation is that the tem of Euler dynamical equations is reduced to the Laplace equation. wever, the solution to the problem of surface wave motion is compli-

cated by
boundar
which is
previous
system (
applicab
on a for
ordinate
Cartesia
coordina
this does
is transfc
must be
culate th
is based c
of the su
was appli
tions (We
for a rela
the conve
wave field

In thi
were simu
Higgins a
(Dold, 19
steepness,
breaking
extremely
expansion
and Sulem
of modula
wave for
methods t

Our g
1-D poten
scales muc
is based o

along regularly located curves, with most of the
es corresponding to free and bound waves. This
the equation $D(\omega/n, k/n) = 0 \quad (n = 1, 2, 3, ...)$,
d by the linear dispersion relation but does not
e k where there is a tendency for the indicated
line. Some other properties of simulated wave
ided temporal evolution of the spectra and spatial
ations. The method developed may be applied to
e assumption of one-dimensionality is acceptable.

numerical solution of the Navier–Stokes
levelopments to geophysical fluid dynam-
models, the long-term evolution of several
mena in different fluids, including the at-
simulated. However, the long-term simu-
de wave field is difficult to perform, since
e Euler equations fail to provide sufficient
rities in wave motion. The main source of
ite difference representation of the vertical
es with different wavenumbers are present.
al investigations of surface gravity waves
ions for potential flow with a free surface.
ermined by the form of the surface and the
ce and in its vicinity. The potential mo-
alizes the phenomenon, since actual wave
turbulent. Fortunately, potential theory
well with observations. For example, it is
heory yields phase velocity estimates with
. A much more sophisticated theory, deal-
interactions (Hasselmann, 1962), which is
otion assumption, gives results which are
ta.

potential motion approximation is that the
ations is reduced to the Laplace equation.
problem of surface wave motion is compli-

cated by the requirement of having to apply the kinematic and dynamic boundary conditions (both nonlinear) on the free surface, the location of which is unknown at any given moment. Some attempts have been made previously to reproduce the evolution of waves in a Cartesian coordinate system (e.g., Prosperetti and Jacobs, 1983), but such techniques are not applicable to long-term integrations. A more feasible approach is based on a formulation of the governing equations in a surface-following coördinate system; the simplest technique uses the difference between the Cartesian vertical coordinate and the surface height as the new vertical coordinate, along with Cartesian coordinates in the horizontal. However, this does not eliminate all of the problems, since the Laplace equation is transformed into a general elliptic equation, and an integral equation must be solved at each time step (Chalikov and Liberman, 1991) to calculate the vertical derivative of the velocity potential. Another approach is based on expanding the velocity potential in power series in the vicinity of the surface. Such a method, developed by Watson and West (1975), was applied to the solution of the two-dimensional potential wave equations (West *et al.*, 1987). Even though this model gave excellent results for a relatively small number of modes, the method is not universal since the convergence of the power series is slow for the case of multi-mode wave fields with typical spectral energy distributions.

In this study we consider only 1-D nonlinear waves. Such waves were simulated numerically with a quasi-Lagrangian technique (Longuet-Higgins and Cokelet, 1976), and with a Cauchy-type integral algorithm (Dold, 1991). The performance of neither scheme was limited by wave steepness, and both were capable of simulating the initial phase of wave breaking (a phenomenon whose later stages are rotational and remain extremely difficult to simulate directly). A method based on a Taylor expansion of the Dirichlet–Neumann operator was developed by Craig and Sulem (1993). The method was illustrated by computing evolution of modulated wave packets and a low order approximation of the Stokes wave for relatively short periods. However, the applicability of these methods to simulating longer time scales is uncertain.

Our goal is to construct a numerical scheme for direct modeling of 1-D potential waves so that the effects of nonlinear interactions on time scales much longer than the wave period may be analyzed. The approach is based on a nonstationary conformal mapping which allows us to rewrite the equations of potential waves (which take into account the effects of capillarity and finite depth) in a surface-following coordinate system, where the Laplace equation retains its form, so that the original system can be represented by two relatively simple evolutionary equations (Section 2). These equations may be solved by using Fourier transform method with high accuracy and computational efficiency. Section 3 deals with stationary solutions of the system; a numerical method to obtain stationary gravity (Stokes) and gravity-capillary waves is presented and results of the computations are discussed. The numerical scheme for the nonstationary equations is described in Section 4. The results of Section 3, as well as mass, momentum and energy conservation criteria, are used for validation of the nonstationary model (Section 5). In Section 6, results of long-term model simulations are discussed, and spectral properties of the obtained wave fields are analyzed.

2. Equations

Consider the principal 2-D equations for potential waves written in Cartesian coordinates, i.e., the Laplace equation for the velocity potential Φ

$$\Phi_{xx} + \Phi_{zz} = 0, \tag{1}$$

and the two boundary conditions at the free surface $z = h(x,t)$: the kinematic condition

$$h_t + h_x \Phi_x - \Phi_z = 0, \tag{2}$$

and the Lagrange integral

$$\Phi_t + \frac{1}{2}\left(\Phi_x^2 + \Phi_z^2\right) + h + p - \sigma h_{xx}(1 + h_x^2)^{-3/2} = 0, \tag{3}$$

where p is the external surface pressure.[1]

The equations are to be solved in the domain

$$-\infty < x < \infty, \quad -H \le z \le h(x,t) \ . \tag{4}$$

The variables Φ and h are considered to be periodic with respect to x , the period being 2π, and a zero normal velocity condition at the bottom is assumed:

$$\Phi_z(x, z = -H, t) = 0. \tag{5}$$

[1] Subscripts of independent variables denote partial differentiation with respect to this variable.

es (which take into account the effects of
n a surface-following coordinate system,
etains its form, so that the original sys-
relatively simple evolutionary equations
nay be solved by using Fourier transform
computational efficiency. Section 3 deals
ie system; a numerical method to obtain
d gravity-capillary waves is presented and
discussed. The numerical scheme for the
scribed in Section 4. The results of Sec-
itum and energy conservation criteria, are
tationary model (Section 5). In Section 6,
ulations are discussed, and spectral prop-
lds are analyzed.

ations for potential waves written in Carte-
ace equation for the velocity potential Φ

$$_{xx} + \Phi_{zz} = 0, \tag{1}$$

ions at the free surface $z = h(x,t)$: the

$$h_x\Phi_x - \Phi_z = 0, \tag{2}$$

$$- h + p - \sigma h_{xx}(1 + h_x^2)^{-3/2} = 0, \tag{3}$$

pressure.[1]

lved in the domain

$$\infty, \quad -H \le z \le h(x,t) \ . \tag{4}$$

nsidered to be periodic with respect to x ,
o normal velocity condition at the bottom

$$, z = -H, t) = 0. \tag{5}$$

ables denote partial differentiation with respect to

Equations (1)–(3) are written in nondimensional form, with the following scales: length L, where $2\pi L$ is the (dimensional) period in the horizontal, time $\mathcal{T} = L^{1/2}g^{-1/2}$, and the velocity potential $L^{3/2}g^{1/2}$ (g– acceleration of gravity). The last term in eqn (3) describes the effect of surface tension, and

$$\sigma = \frac{\Gamma}{g\,L^2} \tag{6}$$

is a nondimensional parameter ($\Gamma \simeq 8 \cdot 10^{-5}\mathrm{m}^3\mathrm{s}^{-2}$ is the kinematic coefficient of surface tension for water).

System (1)–(3) is solved as an initial value problem for the unknown functions Φ and h with given initial conditions $\Phi(x, z = h(x, t = 0), t = 0)$ and $h(x, t = 0)$. However, straightforward numerical integration of this system is known to be computationally inefficient and, for time periods much greater than the time scale $\mathcal{T}$, virtually impracticable. To make a numerical solution feasible, we introduce a surface-following coordinate system which conformally maps the original domain (4) onto the strip

$$-\infty < \xi < \infty, \quad -\tilde{H} \le \zeta \le 0, \tag{7}$$

with a periodicity condition given as

$$\begin{aligned} x(\xi,\zeta,\tau) &= x(\xi + 2\pi, \zeta, \tau) + 2\pi \\ z(\xi,\zeta,\tau) &= z(\xi + 2\pi, \zeta, \tau), \end{aligned} \tag{8}$$

where τ is the new time coordinate, $\tau = t$. (Note that the mapping is time-dependent, since it involves the surface height h.)

It can readily be shown that the required conformal mapping exists and, due to periodicity condition (8), can be represented through Fourier series:

$$x = \xi + x_0(\tau) + \sum_{-M \le k \le M, k \ne 0} \eta_{-k}(\tau) \frac{\cosh k(\zeta + \tilde{H})}{\sinh k\tilde{H}} \vartheta_k(\xi), \tag{9}$$

$$z = \zeta + \eta_0(\tau) + \sum_{-M \le k \le M, k \ne 0} \eta_k(\tau) \frac{\sinh k(\zeta + \tilde{H})}{\sinh k\tilde{H}} \vartheta_k(\xi), \tag{10}$$

where η_k are the coefficients of Fourier expansion of the free surface $\eta(\xi,\tau)$ with respect to the new horizontal coordinate ξ:

$$\eta(\xi,\tau) = h(x(\xi, \zeta = 0, \tau), t = \tau) = \sum_{-M \le k \le M} \eta_k(\tau)\vartheta_k(\xi); \tag{11}$$

denotes the function

$$\vartheta_k(\xi) = \begin{cases} \cos k\xi & k \geq 0 \\ \sin k\xi & k < 0 \end{cases} \tag{12}$$

ote that $(\vartheta_k)_\xi = k\vartheta_{-k}$, and $\sum(A_k\vartheta_k)_\xi = -\sum kA_{-k}\vartheta_k)$; M is the trun-tion number to be used in numerical integration (so far $M = \infty$ is sumed); $x_0(\tau)$ can be chosen arbitrarily, though it is convenient to sume

$$x_0(\tau) = 0. \tag{13}$$

he lower boundary $\zeta = -\tilde{H}$ cannot be chosen arbitrarily, since the lation

$$z(\xi, \zeta = -\tilde{H}, \tau) = -H \tag{14}$$

ust hold, which, after substituting expansion (10), yields:

$$\tilde{H} = H + \eta_0(\tau). \tag{15}$$

nce η_0 is determined by the Fourier expansion (11), and, generally, is unknown function of time, $\tilde{H}$ also depends on time.

ue to the conformity of the mapping, Laplace equation (1) retains its rm in (ξ, ζ) coordinates. Standard derivations show that system (1)–(3) n be written in the new coordinates as follows:

$$\Phi_{\xi\xi} + \Phi_{\zeta\zeta} = 0 \tag{16}$$

$$-z_\xi x_\tau + x_\xi z_\tau = \Phi_\zeta \tag{17}$$

$$\begin{aligned} \Phi_\tau - J^{-1}(x_\xi x_\tau + z_\xi z_\tau)\Phi_\xi + \frac{1}{2}J^{-1}(\Phi_\xi^2 - \Phi_\zeta^2) \\ +z + p - \sigma J^{-3/2}(-x_{\xi\xi}z_\xi + z_{\xi\xi}x_\xi) = 0 \end{aligned} \tag{18}$$

here eqns (17) and (18) are written for the surface $\zeta = 0$ (so that $z = \eta$ represented by expansion (11)), and

$$J = x_\xi^2 + z_\xi^2 = x_\zeta^2 + z_\zeta^2 \tag{19}$$

the Jacobian of the transformation. Boundary condition (5) readily elds:

$$\Phi_\zeta(\xi, \zeta = -\tilde{H}, \tau) = 0. \tag{20}$$

The Laplace
Fourier expa

where ϕ_k are
Thus, eqns (
tions for the
In principle,
tions for the
mulae which

$\Phi_($

$x_\xi(\xi,$

$x_{\xi\xi}(\xi, \zeta$

$x_\tau(\xi, \zeta = 0, \tau$

System (17),
the surface el
value problem

The Laplace equation (16) with boundary condition (20) is solved via Fourier expansion (which reduces system (16) – (18) to a 1-D problem):

$$\Phi = \sum_{-M\le k\le M} \phi_k(\tau)\frac{\cosh k(\zeta+\tilde{H})}{\cosh k\tilde{H}}\vartheta_k(\xi), \tag{21}$$

where ϕ_k are Fourier coefficients of the surface potential $\Phi(\xi,\zeta=0,\tau)$. Thus, eqns (17) and (18) constitute a closed system of prognostic equations for the surface functions $z(\xi,\zeta=0,\tau)=\eta(\xi,\tau)$ and $\Phi(\xi,\zeta=0,\tau)$. In principle, it can be written as a system of ordinary differential equations for the Fourier coefficients η_k, ϕ_k using (11) and the following formulae which are easily obtained from (9), (10), (12), (13), (15), (21):

$$\Phi(\xi,\zeta=0,\tau) = \sum_{-M\le k\le M} \phi_k(\tau)\vartheta_k(\xi) \tag{22}$$

$$\Phi_\xi(\xi,\zeta=0,\tau) = -\sum_{-M\le k\le M} k\phi_{-k}(\tau)\vartheta_k(\xi) \tag{23}$$

$$\Phi_\zeta(\xi,\zeta=0,\tau) = \sum_{-M\le k\le M} k\phi_k(\tau)\tanh\left(k\tilde{H}\right)\vartheta_k(\xi) \tag{24}$$

$$x_\xi(\xi,\zeta=0,\tau) = 1+\sum_{-M\le k\le M, k\neq 0} k\eta_k(\tau)\coth\left(k\tilde{H}\right)\vartheta_k(\xi) \tag{25}$$

$$z_\xi(\xi,\zeta=0,\tau) = -\sum_{-M\le k\le M} k\eta_{-k}(\tau)\vartheta_k(\xi) \tag{26}$$

$$x_{\xi\xi}(\xi,\zeta=0,\tau) = -\sum_{-M\le k\le M, k\neq 0} k^2\eta_{-k}(\tau)\coth\left(k\tilde{H}\right)\vartheta_k(\xi) \tag{27}$$

$$z_{\xi\xi}(\xi,\zeta=0,\tau) = -\sum_{-M\le k\le M} k^2\eta_k(\tau)\vartheta_k(\xi) \tag{28}$$

$$\Phi_\tau(\xi,\zeta=0,\tau) = \sum_{-M\le k\le M} \dot{\phi}_k(\tau)\vartheta_k(\xi) \tag{29}$$

$$x_\tau(\xi,\zeta=0,\tau) = \sum_{-M\le k\le M, k\neq 0} \left(\dot{\eta}_{-k}(\tau)\coth(k\tilde{H}) - \frac{k\eta_{-k}(\tau)\dot{\eta}_0(\tau)}{\sinh^2(k\tilde{H})}\right)\vartheta_k(\xi) \tag{30}$$

$$z_\tau(\xi,\zeta=0,\tau) = \sum_{-M\le k\le M} \dot{\eta}_k(\tau)\vartheta_k(\xi). \tag{31}$$

System (17), (18) is not resolved with respect to the time derivative of the surface elevation $\eta(\xi,\tau)$. During numerical integration of the initial value problem, the values of the time derivative can be obtained with a simple iterative algorithm making use of eqn (17) and Cauchy–Riemann relations $x_{\tau\xi} = z_{\tau\zeta}$, $x_{\tau\zeta} = -z_{\tau\xi}$. However, a more efficient approach may be applied (V. Zakharov, private communication; see also Kuznetsov *et al.*, 1994). Introducing complex variables $\rho = \xi + \mathbf{i}\zeta$ and $r(\rho, \tau) = x(\xi, \zeta, \tau) + \mathbf{i}z(\xi, \zeta, \tau)$, we can rewrite the left-hand side of eqn (17) as follows

$$\operatorname{Im}\left(\frac{r_\tau}{r_\rho}\right)_{\zeta=0} = \left(J^{-1}\Phi_\zeta\right)_{\zeta=0}. \tag{32}$$

Note that due to conformity of the transformation, $r(\rho, \tau)$ is an analytic function of ρ, and so are $r_\tau = x_\tau + \mathbf{i}z_\tau$, $r_\rho = x_\xi + \mathbf{i}z_\xi$, and their ratio in the left-hand side of relation (32). Therefore, if we denote

$$\frac{r_\tau}{r_\rho} = F(\xi, \zeta, \tau) + \mathbf{i}G(\xi, \zeta, \tau), \tag{33}$$

functions F and G are bound by the Cauchy–Riemann relations:

$$F_\xi = G_\zeta, \quad F_\zeta = -G_\xi. \tag{34}$$

Considering that G is a harmonic function of ξ and ζ, and that it becomes zero at the lower boundary $\zeta = -\tilde{H}$ (because at that boundary $z = -H$, $z_\tau = z_\xi = 0$), so that

$$(F + \mathbf{i}G)_{\zeta=-\tilde{H}} = \left(\frac{x_\tau}{x_\xi}\right)_{\zeta=-\tilde{H}} = (F)_{\zeta=-\tilde{H}}, \tag{35}$$

we can write the following expansion:

$$G(\xi, \zeta, \tau) = \sum_{-M\le k\le M, k\ne 0} g_k(\tau)\frac{\sinh k(\zeta + \tilde{H})}{\sinh k\tilde{H}}\vartheta_k(\xi), \tag{36}$$

and relations (34) yield:

$$F(\xi, \zeta, \tau) = f_0(\tau) + \sum_{-M\le k\le M, k\ne 0} g_{-k}(\tau)\frac{\cosh k(\zeta + \tilde{H})}{\sinh k\tilde{H}}\vartheta_k(\xi). \tag{37}$$

Function $f_0(\tau)$ can be found using assumption (13), which together with (33) yields (for any ζ and τ):

$$0 = \int_0^{2\pi} x_\tau \mathrm{d}\,\xi = \int_0^{2\pi}(Fx_\xi - Gz_\xi)\mathrm{d}\xi;$$

ing use of eqn (17) and Cauchy–Riemann
. However, a more efficient approach may
rate communication; see also Kuznetsov
plex variables $\rho = \xi + \mathbf{i}\zeta$ and $r(\rho, \tau) =$
rewrite the left-hand side of eqn (17) as

$$ {}_{\zeta=0} = \left(J^{-1}\Phi_\zeta\right)_{\zeta=0}. \qquad (32)$$

the transformation, $r(\rho, \tau)$ is an analytic
$x_\tau + \mathbf{i}z_\tau$, $r_\rho = x_\xi + \mathbf{i}z_\xi$, and their ratio in
2). Therefore, if we denote

$$,\zeta,\tau) + \mathbf{i}G(\xi,\zeta,\tau), \qquad (33)$$

y the Cauchy–Riemann relations:

$$ G_\zeta, \quad F_\zeta = -G_\xi. \qquad (34)$$

c function of ξ and ζ, and that it becomes
$-\tilde{H}$ (because at that boundary $z = -H$,

$$ = \left(\frac{x_\tau}{x_\xi}\right)_{\zeta=-\tilde{H}} = (F)_{\zeta=-\tilde{H}}, \qquad (35)$$

nsion:

$$ {}_{,k\neq 0} \; g_k(\tau)\frac{\sinh k(\zeta+\tilde{H})}{\sinh k\tilde{H}}\vartheta_k(\xi), \qquad (36)$$

$$ {}_{M,k\neq 0} \; g_{-k}(\tau)\frac{\cosh k(\zeta+\tilde{H})}{\sinh k\tilde{H}}\vartheta_k(\xi). \qquad (37)$$

ng assumption (13), which together with

$$ = \int_0^{2\pi}(Fx_\xi - Gz_\xi)\mathrm{d}\xi;$$

substituting expansions (36), (37), (9), (10), and integrating the products of the Fourier series, we obtain:

$$f_0 = \frac{1}{2}\sum_{-M\leq k\leq M, k\neq 0} k\eta_{-k}g_k \sinh^{-2}(k\tilde{H}). \qquad (38)$$

Then if

$$g(\xi,\tau) = G(\xi,\zeta=0,\tau) = \sum_{-M\leq k\leq M, k\neq 0} g_k(\tau)\vartheta_k(\xi) \qquad (39)$$

is known,

$$f(\xi,\tau) = F(\xi,\zeta=0,\tau) = f_0(\tau) + \sum_{-M\leq k\leq M, k\neq 0} g_{-k}(\tau)\coth(k\tilde{H})\vartheta_k(\xi) \qquad (40)$$

is also known: f is a generalization of the Hilbert transform of g, which, for $k \neq 0$, may be defined in Fourier space as

$$f_k = g_{-k}\coth(k\tilde{H}), \quad g_k = -f_{-k}\tanh(k\tilde{H}), \qquad (41)$$

whereas $g_0 = 0$ and f_0 is defined by (38). Thus, we can replace eqn (17) by explicit expressions for the time derivatives x_τ and z_τ which follow from (33). Finally, eqns (17) and (18) can be rewritten as a system which is resolved with respect to the time derivatives (here $\zeta = 0$):

$$z_\tau = x_\xi g + z_\xi f \qquad (42)$$

$$\Phi_\tau = f\Phi_\xi - \frac{1}{2}J^{-1}(\Phi_\xi^2 - \Phi_\zeta^2) - z - p + \sigma J^{-3/2}(-x_{\xi\xi}z_\xi + z_{\xi\xi}x_\xi), \qquad (43)$$

where according to (32),

$$g = \left(J^{-1}\Phi_\zeta\right)_{\zeta=0}, \qquad (44)$$

f is obtained from g according to (38)–(40), and the derivatives can be expressed through Fourier series (22)–(29), (31) (expansion (30) is no longer needed, since x_τ has been eliminated from the system).

Thus, the original system of equations is transformed into two evolutionary equations (42), (43) which can be effectively solved using the Fourier transform method (see Section 4).

For deep water ($H = \infty$), the coefficients in expansions (24), (25),), (30), (38), (40), (41) become simpler, since $\tanh(k\tilde{H})$ and $\coth(k\tilde{H})$ replaced by $\mathrm{sign}(k)$, and the terms with $\sinh^{-2}(k\tilde{H})$ vanish. In par- ılar, operator (41) becomes a conventional Hilbert transform, and (38) educed to $f_0 = 0$.

To include the case of pure capillary waves, it is convenient to use ifferent scaling: $L^{3/2}\Gamma^{-1/2}$ for time and $L^{1/2}\Gamma^{1/2}$ for velocity poten- . With the new nondimensional variables, eqns (43), (42) acquire the owing form:

$$z_\tau = x_\xi g + z_\xi f \tag{45}$$

$$\Phi_\tau = f\Phi_\xi - \frac{1}{2}J^{-1}(\Phi_\xi^2 - \Phi_\zeta^2) - \alpha z - p + J^{-3/2}(-x_{\xi\xi}z_\xi + z_{\xi\xi}x_\xi), \tag{46}$$

re $\alpha = \sigma^{-1}$.

Stationary solutions

the stationary problem, the method of conformal mapping is a well- wn approach based on using the velocity potential Φ and the stream tion Ψ as the independent variables (e.g. Crapper, 1984). It is easy how that in this case

$$\Phi = -c\xi + \Phi_0, \quad \Psi = c\zeta + \Psi_0, \tag{47}$$

re $-c$ is the velocity of the mean flow, $\Phi_x = -\Psi_z$ and $\Phi_z = \Psi_x$ are the zontal and the vertical Cartesian velocity components respectively, Φ_0 and Ψ_0 are constants.

For the stationary version of system (1)–(3) (or (16)–(18)) to describe ressive waves, the periodicity condition on Φ, which implies a zero n flow velocity, must be replaced by the weaker condition of period- of the velocity components, i.e., of the spatial derivatives of Φ. In a dinate system moving with the wave's phase velocity c, the mean flow city is equal to $-c$, and the velocity potential Φ is given by relations where Φ_0 must be allowed to depend on time (since stationarity is med for the velocity field rather than the velocity potential). Con- ently, with the external pressure $p = 0$, system (16)–(18) is reduced ne equation written for the surface $\zeta = 0$:

$$\frac{1}{2}c^2J^{-1} + z - \sigma J^{-3/2}(-x_{\xi\xi}z_\xi + z_{\xi\xi}x_\xi) = a \tag{48}$$

where $a =$
on time, a i
linear).

In this w
(9), (10) for
The nonline
ing the tota
(1970) and I
is discussed

Note tha
ential order,
had to deve
gravity-capil
numerical sc

Below we
generalizatio
straightforw

3.1 Pure g

With $\sigma = 0$,
on expansion
series of the
1880) who i
recent studie
oriented recu
coefficients;
tions up to 1

Here, the
surface heigh
conformal m
by the coeffi

:oefficients in expansions (24), (25),
npler, since $\tanh(k\tilde{H})$ and $\coth(k\tilde{H})$
ms with $\sinh^{-2}(k\tilde{H})$ vanish. In par-
'entional Hilbert transform, and (38)

llary waves, it is convenient to use
ne and $L^{1/2}\Gamma^{1/2}$ for velocity poten-
ariables, eqns (43), (42) acquire the

$$\ldots + z_\xi f \quad (45)$$

$$- p + J^{-3/2}(-x_{\xi\xi}z_\xi + z_{\xi\xi}x_\xi), \quad (46)$$

ıod of conformal mapping is a well-
velocity potential Φ and the stream
les (e.g. Crapper, 1984). It is easy

$$\Psi = c\zeta + \Psi_0, \quad (47)$$

ow, $\Phi_x = -\Psi_z$ and $\Phi_z = \Psi_x$ are the
velocity components respectively,

n (1)–(3) (or (16)–(18)) to describe
ıdition on Φ, which implies a zero
by the weaker condition of period-
of the spatial derivatives of Φ. In a
ve's phase velocity c, the mean flow
ty potential Φ is given by relations
oend on time (since stationarity is
than the velocity potential). Con-
$= 0$, system (16)–(18) is reduced
e $\zeta = 0$:

$$-x_{\xi\xi}z_\xi + z_{\xi\xi}x_\xi) = a \quad (48)$$

where $a = -\frac{d\Phi_0}{d\tau}$, and since the left-hand side of (48) does not depend on time, a is a constant (so that the dependence of Φ_0 on τ may only be linear).

In this work, eqn (48) is solved numerically using Fourier expansions (9), (10) for x and z and (25)–(28) for the derivatives in (48) and (19). The nonlinearities are evaluated at gridpoints $\xi^{(j)} = 2\pi(j-1)/N$, N being the total number of gridpoints. This approach, developed by Orszag (1970) and Eliassen *et al.* (1970), is known as the transform method and is discussed in more detail in Section 4.

Note that because σ is a factor in a term having the highest differential order, we may face effects of singularity for small σ. Indeed, we had to develop two different schemes for the cases of pure gravity and gravity-capillary waves, and it will be seen that in the latter case the numerical solution does not approach a Stokes wave as σ decreases.

Below we consider only the case of deep water ($H = \infty$); however, generalization of the algorithms described in the following subsections is straightforward for the case of a finite depth.

3.1 Pure gravity waves

With $\sigma = 0$, the solutions of eqn (48) are Stokes waves. A method based on expansion of the Fourier coefficients of the surface height in power series of the wave amplitude was initially proposed by Stokes (1847, 1880) who in his latter work obtained a fifth-order approximation. In recent studies, the method has been further developed into a computer-oriented recursive scheme which produces consecutive power expansion coefficients; Drennan *et al.* (1992) carried out the power series calculations up to 170 terms.

Here, the solutions in the form of Fourier expansion coefficients for the surface height were sought numerically with an iterative algorithm. The conformal mapping with surface boundary condition (48) is determined by the coefficients η_k through the relationships

$$x(\xi, \zeta) = \xi + \sum_{-M \le k \le M, k \ne 0} \eta_{-k} \exp(k\zeta) \vartheta_k(\xi) \quad (49)$$

$$z(\xi,\zeta) = \zeta + \sum_{-M\le k\le M} \eta_k \exp(k\zeta)\vartheta_k(\xi) \qquad (50)$$

the stationary deep-water versions of expansions (9), (10).), formulae (49), (50) may serve as a parametric representa-surface.

G3. Let

$a =$

This will ensure rel gridpoint values of

$\log J^{[n+1]}$

where $()_0$ denotes n

G4. Find the Fouri $n = n+1$ and retur

e gravity waves, eqn (48) can be rewritten in the form

$$\log\left(\frac{1}{2}c^2\right) - \log J = \log(a - z). \qquad (51)$$

$= \log \frac{\mathrm{d}\, r}{\mathrm{d}\, \rho}$ with r, ρ defined as in (32), it can be seen that

$$\log J = 2\mathrm{Re}(w), \quad z_\xi = \mathrm{Im}\ (\exp w). \qquad (52)$$

e Fourier expansion for $\log J$ is known, $\mathrm{Im}(w)$ (also in the ce) can be found via the Hilbert transform as in the second of es (41), after which w and then $\exp w$ can be calculated at the This yields z_ξ, and after finding the corresponding Fourier by direct Fourier transform, z can be obtained by integration space. Thus, z can be easily found if $\log J$ is known. This reduce the differential relationship (51) to an equation with operator, which may be solved by a simple iterative procedure.

ıg that z is an even function of ξ , it is convenient to choose

$$s = \frac{1}{4}\left(\log J(\xi = 0, \zeta = 0) - \log J(\xi = \pi, \zeta = 0)\right) \qquad (53)$$

meter determining the amplitude of the wave (in linear ap-ı, s is equal to the amplitude). With $\chi^{[n]}$ denoting the value ble χ on nth iteration, the scheme can be written as follows:

e $n = 0$, $\log J^{[0]} = 2s\ \mathrm{e}^\zeta \cos\xi$ (this is the solution of the lin-blem).

en $\log J^{[n]}$, use Hilbert transform (41), complex exponent cal-d integration in Fourier space to find $z^{[n]}$ as described above. mum surface gridpoint value of $\mid z^{[n]} - z^{[n-1]} \mid$ is less than ed accuracy ϵ, the iterations are completed, and $z^{[n]}$ is an e solution within the accuracy given.

The last term in iteration: in accorda Equality (54) is bas is zero, which follo $\zeta \to -\infty$.

Figure 1 illustra 384, $N = 1728$, $\epsilon =$ profiles are 0.04, 0.0 from 28 for $s = 0.04$

$A = \frac{1}{2}(\eta(\xi$

is approximately 0.4 imum steepness (ab

Theoretically, s wave whose crest co with $J(\xi = 0, \zeta = 0$ much larger than th close to that of the down dramatically, the accuracy of the for large s the num values of M, N ind

G3. Let

$$a = a^{[n+1]} = \frac{e^{4s} z^{[n]}(\xi = 0) - z^{[n]}(\xi = \pi)}{e^{4s} - 1}.$$

This will ensure relation (53) for the next iteration. Calculate sufrace gridpoint values of

$$\log J^{[n+1]} = -\log(a^{[n+1]} - z^{[n]}) + (\log(a^{[n+1]} - z^{[n]}))_0 \qquad (54)$$

where $()_0$ denotes mean over ξ , i.e. 0th Fourier coefficient.

G4. Find the Fourier expansion of $\log J^{[n+1]}$ by a Fourier transform; let $n = n + 1$ and return to step G2.

The last term in (54) allows us to find the phase velocity on $(n+1)$-st iteration: in accordance with eqn (51), this term is equal to $\log\left(\frac{1}{2}(c^{[n+1]})^2\right)$. Equality (54) is based on the fact that the mean value of $\log J$ over ξ is zero, which follows from the first of relations (52), as $w \to 0$ when $\zeta \to -\infty$.

Figure 1 illustrates some results of the described procedure for $M = 384$, $N = 1728$, $\epsilon = 10^{-11}$. The values of the parameter s for the given profiles are 0.04, 0.08, 0.16, 0.32, 1.06. The number of iterations varied from 28 for $s = 0.04$ to 44 for $s = 1.06$. For $s = 1.06$, the amplitude

$$A = \frac{1}{2}(\eta(\xi = 0) - \eta(\xi = \pi)) = \frac{1}{2}(h(x = 0) - h(x = \pi)) \qquad (55)$$

is approximately 0.4374 which is close to that of Stokes wave with maximum steepness (about 0.443 according to Longuet-Higgins, 1975).

Theoretically, s can be arbitrarily large; $s = \infty$ for the steepest Stokes wave whose crest constitutes an angle of 120° and thus is a singularity with $J(\xi = 0, \zeta = 0) = \infty$. The algorithm does converge for values of s much larger than those used in Fig. 1; however, when the profile becomes close to that of the steepest wave, convergence of the Fourier series slows down dramatically, and at the same time, due to strong nonlinearities, the accuracy of the transform method decreases sharply. As a result, for large s the numerical solution contains spurious oscillations; with the values of M, N indicated above, for $s > 1.06$, the maximum slope of the ned profile exceeds 30°, which is a theoretical maximum.

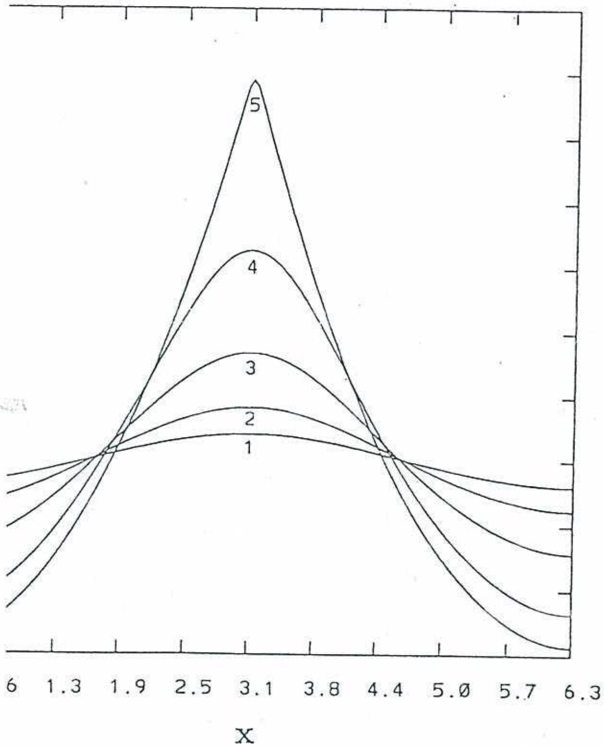

Stokes waves: Curve 1 – A = 0.0399, 2 – A = 0.0793, 3 – 0.2806, 5 – A = 0.4374.

tion convergence criterium ϵ is small enough, the error he truncation error, which can be evaluated by com- btained with different resolutions. Such a comparison r three resolutions: M = 384, N = 1728; M = 192, 6, N = 432. The results are illustrated in Table 1, alue of the amplitude A (as defined in (55)) obtained n number M; $MAXD_{M_1,M_2}$ is the maximum gridpoint nce

$$= \left((x_{M_1} - x_{M_2})^2 + (z_{M_1} - z_{M_2})^2\right)^{1/2}, \qquad (56)$$

) , $z_M = z_M(\xi)$ is the numerical solution for x, z at

$\zeta = 0$ obtained with the t

$$RMSD_{M_1,M}$$

is the root mean square d

Table 1 shows that for very small for all tested re M; the convergence decel the steepest wave. For all the wave's crest.

Table 1: Comparison of Stokes tions

s	A
0.4	0.32
0.6	0.39
0.8	0.42
1.0	0.43
1.2	0.43
1.8	0.44
2.0	0.43

s	$RMSD_{96,384}$	RM
0.4	$1.3 \cdot 10^{-12}$	1.5
0.6	$3.9 \cdot 10^{-6}$	3.0
0.8	$4.8 \cdot 10^{-4}$	3.0
1.0	$3.0 \cdot 10^{-3}$	6.7
1.2	$6.8 \cdot 10^{-3}$	2.2
1.8	$2.1 \cdot 10^{-2}$	7.6
2.0	$2.6 \cdot 10^{-2}$	9.7

3.2 Gravity-capillary w

An iterative algorithm sim out to obtain numerical sol which is a theoretical maximum.

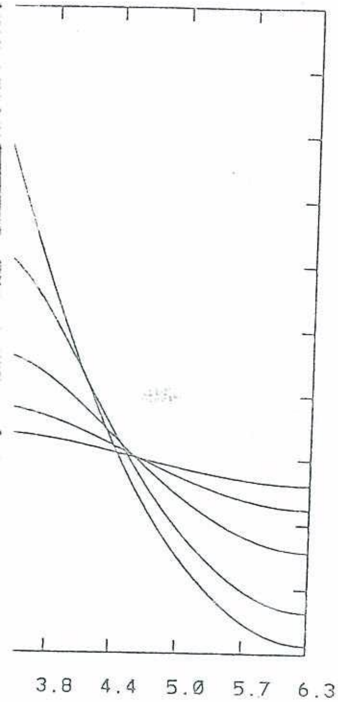

A = 0.0399, 2 − A = 0.0793, 3 −

m ϵ is small enough, the error ich can be evaluated by com- esolutions. Such a comparison = 384, N = 1728; M = 192, lts are illustrated in Table 1, (as defined in (55)) obtained $_{,M_2}$ is the maximum gridpoint

$$- z_{M_2})^2\Big)^{1/2}, \qquad (56)$$

umerical solution for x, z at

$\zeta = 0$ obtained with the truncation number M;

$$RMSD_{M_1,M_2} = \left(\frac{1}{2\pi}\int_0^{2\pi}(R(\xi))^2 \mathrm{d}(x(\xi))\right)^{1/2} \qquad (57)$$

is the root mean square difference over x coordinate.

Table 1 shows that for amplitudes $A < 0.4$ the truncation errors are very small for all tested resolutions and decrease rapidly with increasing M; the convergence decelerates when the amplitude approaches that of the steepest wave. For all examples, the maximum error was located near the wave's crest.

Table 1: Comparison of Stokes wave profiles calculated with different spectral resolutions

s	A_{384}	$A_{96} - A_{384}$	$A_{192} - A_{384}$
0.4	0.3273	$4.2 \cdot 10^{-13}$	$1.6 \cdot 10^{-15}$
0.6	0.3986	$1.5 \cdot 10^{-6}$	$1.1 \cdot 10^{-9}$
0.8	0.4264	$8.3 \cdot 10^{-5}$	$3.2 \cdot 10^{-6}$
1.0	0.4360	$-1.4 \cdot 10^{-4}$	$-1.2 \cdot 10^{-4}$
1.2	0.4394	$-1.1 \cdot 10^{-3}$	$-1.3 \cdot 10^{-3}$
1.8	0.4405	$-5.5 \cdot 10^{-3}$	$-3.0 \cdot 10^{-3}$
2.0	0.4393	$-6.9 \cdot 10^{-3}$	$-3.9 \cdot 10^{-3}$

s	$RMSD_{96,384}$	$RMSD_{192,384}$	$MAXD_{96,384}$	$MAXD_{192,384}$
0.4	$1.3 \cdot 10^{-12}$	$1.5 \cdot 10^{-15}$	$3.7 \cdot 10^{-12}$	$2.2 \cdot 10^{-15}$
0.6	$3.9 \cdot 10^{-6}$	$3.0 \cdot 10^{-8}$	$1.7 \cdot 10^{-5}$	$1.3 \cdot 10^{-8}$
0.8	$4.8 \cdot 10^{-4}$	$3.0 \cdot 10^{-5}$	$2.3 \cdot 10^{-3}$	$1.7 \cdot 10^{-4}$
1.0	$3.0 \cdot 10^{-3}$	$6.7 \cdot 10^{-4}$	$1.1 \cdot 10^{-2}$	$3.3 \cdot 10^{-3}$
1.2	$6.8 \cdot 10^{-3}$	$2.2 \cdot 10^{-3}$	$2.1 \cdot 10^{-2}$	$9.3 \cdot 10^{-3}$
1.8	$2.1 \cdot 10^{-2}$	$7.6 \cdot 10^{-3}$	$4.9 \cdot 10^{-2}$	$2.6 \cdot 10^{-2}$
2.0	$2.6 \cdot 10^{-2}$	$9.7 \cdot 10^{-3}$	$5.9 \cdot 10^{-2}$	$3.1 \cdot 10^{-2}$

3.2 Gravity-capillary waves

An iterative algorithm similar to that described above has been worked out to obtain numerical solutions of eqn (48) with $\sigma > 0$. Here, we again

:e height is an even function of x, and hence of ξ.

;orithm it is convenient to rewrite eqn (48) in the

$$\frac{\alpha}{+1}z - a_\star\Big) - \frac{1}{\alpha+1}J^{-1}(-x_{\xi\xi}z_\xi + z_{\xi\xi}x_\xi) = 0 \quad (58)$$

$a\alpha/(\alpha+1)$; $c_\star^2 = c^2\alpha/(\alpha+1) = c^2/(1+\sigma)$. Note the actual phase velocity to the phase velocity of

$$= \left(\frac{1}{k} + \sigma k\right)^{1/2} = \left(\frac{1}{k} + \frac{k}{\alpha}\right)^{1/2} \quad (59)$$

1; the convenience of representing the results in :hat it does not depend on the choice of the time

;t term on the left-hand side of eqn (58), it can be

$$z_{\xi\xi}x_\xi) = \mathrm{Im}\left(\frac{\mathrm{d}w}{\mathrm{d}\rho}\right) = \mathrm{Im}(w_\xi) = (\mathrm{Im}\ \ w)_\xi \quad (60)$$

he same meaning as in relations (52). Also, if we of the surface height over the x coordinate is zero, the following choice of the 0th Fourier coefficient:

$$\eta_0 = -\frac{1}{2}\sum_{1\le k<M} k\eta_k^2, \quad (61)$$

d $c_\star$ are bound by the relationship:

$$a_\star = \frac{1}{2}c_\star^2. \quad (62)$$

ɜs, this property directly follows from results by 5); for the general case of gravity-capillary waves, s, as it can be deduced from the observation that ary term in eqn (3) over x is zero.

Relations (60), (62) and (5

$$-2(\alpha+1)a_\star \sinh(\mathrm{R}$$

Choosing

$$S = -\frac{1}{2}(\mathrm{Im}\ w_\xi(\xi =$$

as the parameter determining it is equal to the amplitude fo mulate the iteration scheme as

GC1. Assume $n = 0$, $(\mathrm{Im}\ w)_\xi^{[0}$ linearized problem).

GC2. For given $(\mathrm{Im}\ w)_\xi^{[n]}$, and a Hilbert transform (as in at each gridpoint, then find $z^{[}$ according to the second relati termined by relation (61). If $\mid z^{[n]} - z^{[n-1]} \mid$ is less than the completed, and $z^{[n]}$ is an appro

GC3. Calculate surface values eqn (63), by substituting $w =$ Similarly to step G3, $a_\star = a_\star^{[}$ holds for $w = w^{[n+1]}$:

$$a_\star^{[n+1]} = \frac{\alpha}{2(\alpha+1)}\frac{\eta^{[n]}(0)\ \mathrm{e}}{\mathrm{si}}$$

where

$$\eta^{[n]}(\xi) = z^{[n]}(\xi, \zeta = ($$

GC4. Find the Fourier expans let $n = n+1$ and return to ste

Convergence of the algorith on the parameter S for differe the wave profiles obtained for

$$\hat{A} = \frac{1}{2}\left(\mathrm{Max}_{0\le j\le N}\eta(\xi\right.$$

Relations (60), (62) and (52) allow us to rewrite eqn (58) as follows:

$$-2(\alpha+1)a_* \sinh(\mathrm{Re}\, w) + \alpha \exp(\mathrm{Re}\, w) z = (\mathrm{Im}\, w)_\xi. \qquad (63)$$

Choosing

$$S = -\frac{1}{2}(\mathrm{Im}\, w_\xi(\xi=0, \zeta=0) - \mathrm{Im}\, w_\xi(\xi=\pi, \zeta=0)) \qquad (64)$$

as the parameter determining the wave amplitude (like s in relation (53), it is equal to the amplitude for the linearized problem), we can now formulate the iteration scheme as follows:

GC1. Assume $n=0$, $(\mathrm{Im}\, w)_\xi^{[0]} = -Se^\zeta \cos\xi$ (this is the solution of the linearized problem).

GC2. For given $(\mathrm{Im}\, w)_\xi^{[n]}$, find $w^{[n]}$ in Fourier space by integration and a Hilbert transform (as in the first of equalities (41)); find $\exp(w^{[n]})$ at each gridpoint, then find $z^{[n]}$ by a Fourier transform and integration according to the second relation (52), with the integration constant determined by relation (61). If the maximum surface gridpoint value of $\mid z^{[n]} - z^{[n-1]} \mid$ is less than the prescribed accuracy ϵ, the iterations are completed, and $z^{[n]}$ is an approximate solution within the accuracy given.

GC3. Calculate surface values of $(\mathrm{Im}\, w)_\xi^{[n+1]}$ as the right-hand side of eqn (63), by substituting $w = w^{[n]}$, $z = z^{[n]}$ into the left-hand side. Similarly to step G3, $a_* = a_*^{[n+1]}$ must be chosen so that relation (64) holds for $w = w^{[n+1]}$:

$$a_*^{[n+1]} = \frac{\alpha}{2(\alpha+1)} \frac{\eta^{[n]}(0)\exp(R^{[n]}(0)) - \eta^{[n]}(\pi)\exp(R^{[n]}(\pi))}{\sinh(R^{[n]}(0)) - \sinh(R^{[n]}(\pi))} \qquad (65)$$

where

$$\eta^{[n]}(\xi) = z^{[n]}(\xi, \zeta=0)\ , \quad R^{[n]}(\xi) = \mathrm{Re}\, w^{[n]}(\xi, \zeta=0).$$

GC4. Find the Fourier expansion of $(\mathrm{Im}\, w)_\xi^{[n+1]}$ by a Fourier transform; let $n = n+1$ and return to step GC2.

Convergence of the algorithm and the dependence of wave amplitude on the parameter S for different α are characterized by Table 2. Since the wave profiles obtained for large α have two maxima, values of

$$\hat{A} = \frac{1}{2}\left(\mathrm{Max}_{0\le j\le N}\eta(\xi=\xi^{(j)}) - \mathrm{Min}_{0\le j\le N}\eta(\xi=\xi^{(j)})\right) \qquad (66)$$

ι A (relation (55)). The calculations were per- $= 432$, $\epsilon = 10^{-11}$.

nbers of iterations N_{it} for gravity-capillary waves calcu- Blank entries mean that the scheme failed to converge

0.1	0.2	0.4	0.6	0.8	1
1000	0.2000	0.4000	0.6000	0.8000	1.0000
1000	0.2000	0.4000	0.6000	0.8000	1.0000
16	18	20	21	21	20
)996	0.1969	0.3772	0.5315	0.6583	0.7606
)996	0.1969	0.3772	0.5315	0.6583	0.7606
41	41	39	39	43	43
)971	0.1814	0.3109	0.4066	0.4815	0.5420
)971	0.1814	0.3109	0.4066	0.4815	0.5420
61	48	47	44	43	42
)880	0.1497	0.2382	0.3050	0.3593	0.4049
)880	0.1497	0.2382	0.3050	0.3593	0.4049
93	58	48	43	41	39
)655	0.1090	0.1760	0.2291	0.2738	
)711	0.1165	0.1844	0.2375	0.2819	
157	81	44	41	40	
)262	0.0512	0.0967	0.1361		
)895	0.1064	0.1417	0.1750		
106	88	62	54		
)162	0.0323	0.0636			
)853	0.0955	0.1182			
134	122	97			
)124	0.0247	0.0490			
)653	0.0742	0.0946			
178	157	138			
)109					
)247					
2051					

$= 0.1$, samples of calculated wave profiles with Figs 2 and 3, respectively. These results were ation of the algorithm above, which, more con-

veniently, uses $\hat{A}$ instead of S a vantage of the modified version $(\alpha, \hat{A})$ plane is notably larger tha however, computationally it is le nested calculations to numerical tion, while in step GC3 $a_\star$ is rea

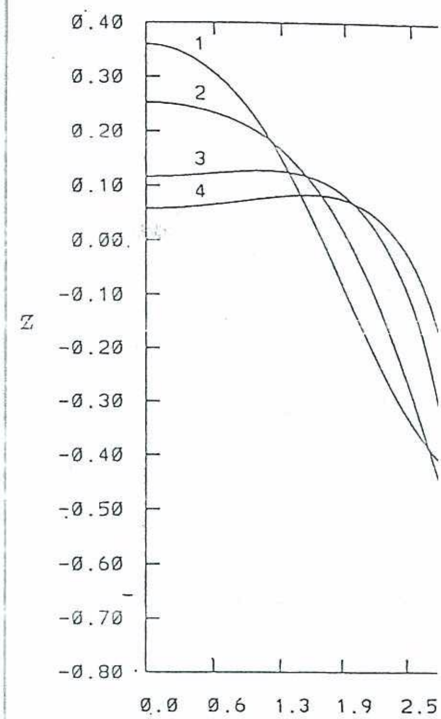

Figure 2: Profiles of gravity-capillary wave), $2 - \alpha = 1$, $3 - \alpha = 2$, $4 - \alpha = 3$

From Table 2 and Figs 2 anc α (i.e., with the capillarity coeffi not approach those of pure gravit smaller scales where capillarity ε with $\alpha = 2$, two maxima emerge, (the absolute minimum being al

5[illegible])). The calculations were per-
-[illegible].

[illegible] N_{it} for gravity-capillary waves calcu-
[illegible] that the scheme failed to converge

0.4	0.6	0.8	1
[illegible].4000	0.6000	0.8000	1.0000
[illegible].4000	0.6000	0.8000	1.0000
20	21	21	20
[illegible].3772	0.5315	0.6583	0.7606
[illegible].3772	0.5315	0.6583	0.7606
39	39	43	43
[illegible].3109	0.4066	0.4815	0.5420
[illegible].3109	0.4066	0.4815	0.5420
47	44	43	42
[illegible].2382	0.3050	0.3593	0.4049
[illegible].2382	0.3050	0.3593	0.4049
48	43	41	39
[illegible].1760	0.2291	0.2738	
[illegible].1844	0.2375	0.2819	
44	41	40	
[illegible].0967	0.1361		
.1417	0.1750		
62	54		
.0636			
.1182			
97			
.0490			
.0946			
138			

[illegible] calculated wave profiles with
[illegible]espectively. These results were
[illegible]rithm above, which, more con-

veniently, uses $\hat{A}$ instead of S as a wave parameter. An important advantage of the modified version is that its domain of convergence in the $(\alpha, \hat{A})$ plane is notably larger than that of the original scheme GC1–GC4; however, computationally it is less efficient than the latter, as it requires nested calculations to numerically determine values of a_* for each iteration, while in step GC3 a_* is readily yielded by formula (65).

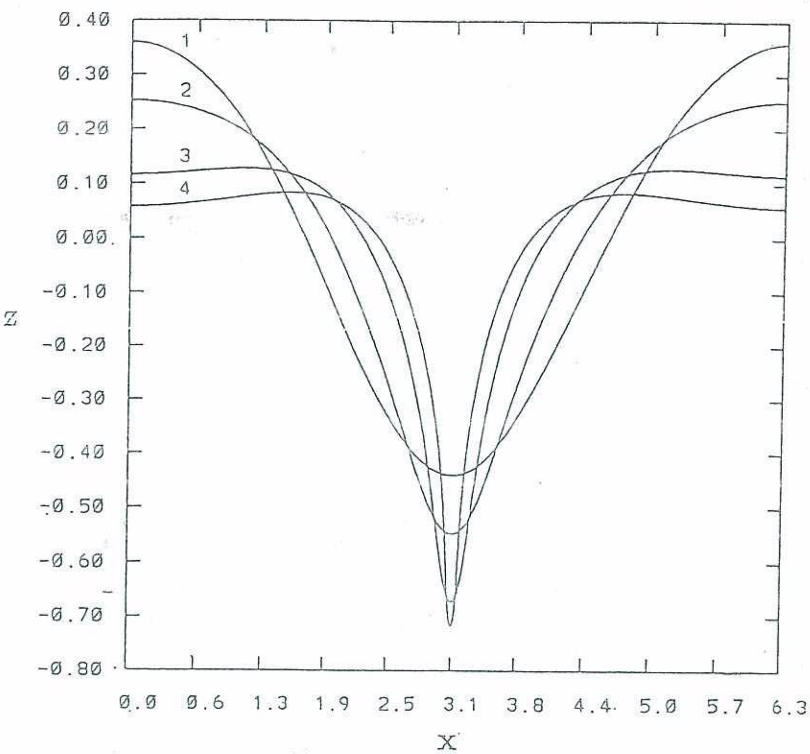

Figure 2: Profiles of gravity-capillary waves, $\hat{A} = 0.4$. Curve 1 – $\alpha = 0$ (Crapper's wave), 2 – $\alpha = 1$, 3 – $\alpha = 2$, 4 – $\alpha = 3$.

From Table 2 and Figs 2 and 3, it can be seen that with increasing α (i.e., with the capillarity coefficient σ decreasing), the wave profiles do not approach those of pure gravity waves, but rather shift their energy to smaller scales where capillarity effects are more pronounced. Beginning with $\alpha = 2$, two maxima emerge, so that $x = 0$ becomes a local minimum (the absolute minimum being always at $x = \pi$); at the same time the

of convergence decreases rapidly, especially for small amplitudes
or those values of α which ensure equal linear phase velocities (59)
o neighboring wavenumbers k, $k+1$, namely $\alpha = 2$ $(k = 1)$ and
$(k = 2)$.

ither the scheme GC1–GC4 nor its aforementioned modification
rged with $\alpha > 6$; however, the modified scheme converged for $\hat{A}$
considerably larger than those indicated in Table 2.

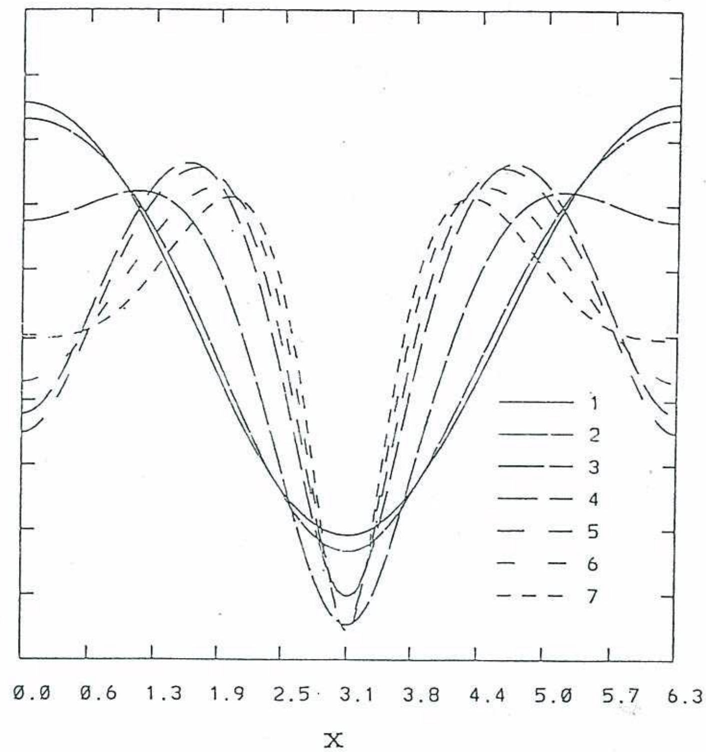

3: Profiles of gravity-capillary waves, $\hat{A} = 0.1$. Curve 1 – $\alpha = 0$ (Crapper's
2 – $\alpha = 1$, 3 – $\alpha = 2$, 4 – $\alpha = 3$, 5 – $\alpha = 4$, 6 – $\alpha = 5$, 7 – $\alpha = 6$.

e dependence of the normalized phase velocity $c_\star$ on $\sigma = 1/\alpha$, as
ated by Fig. 4, is consistent with the behavior of the corresponding
s. When σ decreases but remains positive, $c_\star$ decreases and does
proach its value at sigma=0. The latter is always greater than 1

and, except fo
increasing fun
function of $\hat{A}$
phase velocity
minimum valu

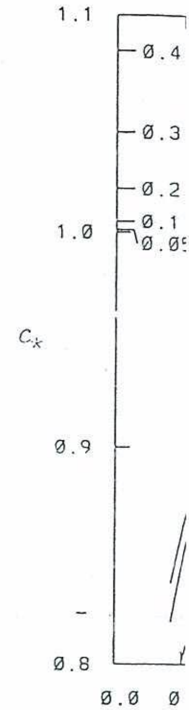

Figure 4: Norma
capillarity coeffic

For most c
with results ob
maximum diffe
ceeded $1.2 \cdot 10$

y, especially for small amplitudes
e equal linear phase velocities (59)
$k+1$, namely $\alpha = 2$ ($k = 1$) and

r its aforementioned modification
modified scheme converged for $\hat{A}$
ndicated in Table 2.

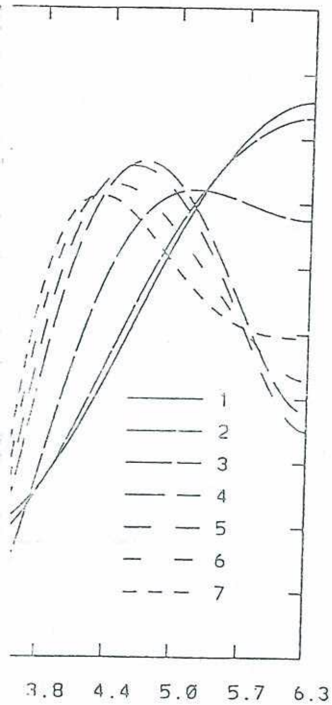

$\hat{A} = 0.1$. Curve 1 – $\alpha = 0$ (Crapper's
$= 4$, 6 – $\alpha = 5$, 7 – $\alpha = 6$.

phase velocity c_* on $\sigma = 1/\alpha$, as
the behavior of the corresponding
s positive, c_* decreases and does
e latter is always greater than 1

and, except for a small interval in the vicinity of the maximum $\hat{A}$, is an increasing function of $\hat{A}$, while for $\sigma \neq 0$ the calculated c_* is a decreasing function of $\hat{A}$ and always less than 1. In fact, for small values of $\hat{A}$, the phase velocity corresponding to a given σ turns out to be close to the minimum value of c_l (relation (59)) over k.

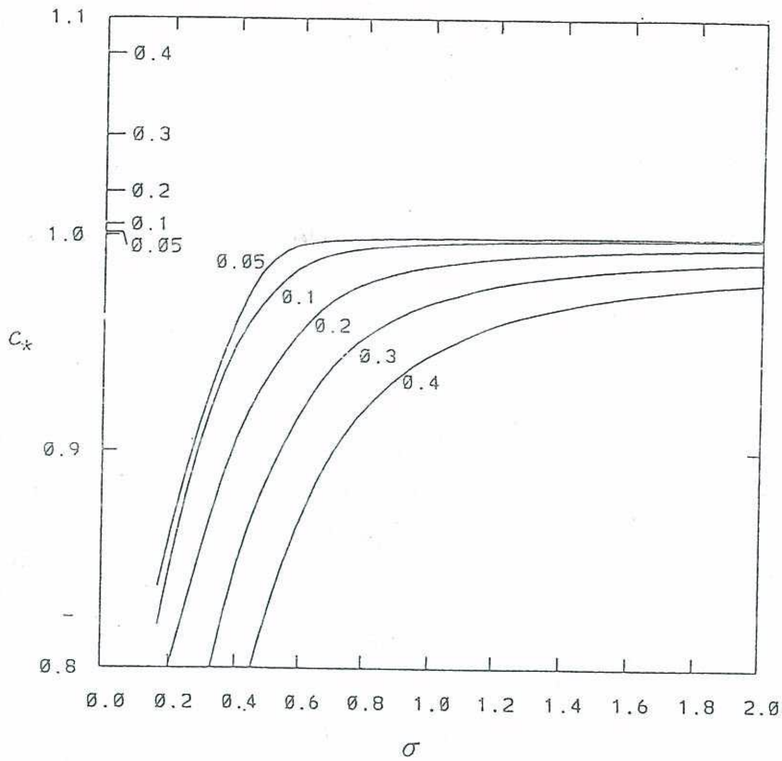

Figure 4: Normalized phase velocity $c_* = c/\sqrt{1+\sigma}$ as a function of nondimensional capillarity coefficient σ. Wave amplitudes A are indicated at the respective curves.

For most cases represented in Table 2, a comparison was performed with results obtained for a higher resolution ($M = 384$, $N = 1728$). The maximum difference between surface profiles as defined in (56) never exceeded $1.2 \cdot 10^{-11}$, which means that the truncation errors are negligible.

illary waves

ary waves, which are described by eqn (58) if we formally
ɜ solution is represented by a simple formula (Crapper,
ıotation, it can be written as

$$x(\xi,\zeta) = \xi + \frac{4q\sin\xi}{1-2q\cos\xi+q^2}, \tag{67}$$

$$z(\xi,\zeta) = \zeta + \frac{4q(\cos\xi - q)}{1-2q\cos\xi+q^2} - \frac{1}{2}A^2, \tag{68}$$

$$q = be^{\zeta}, \quad b = \frac{-2+\sqrt{4+A^2}}{A}, \tag{69}$$

ɔ, c_*, a_* are bound by the following relationships:

$$= \hat{A} = S = \frac{4b}{1-b^2}, \quad \frac{1}{2}c_*^2 = a_* = \frac{1}{\sqrt{4+A^2}}. \tag{70}$$

n (68) may be any constant but here it is chosen to satisfy

ion (67)–(70) was used as another means to validate scheme
h $\alpha = 0$. For all tested amplitudes, up to the maximum
tude (e.g., Crapper, 1984), the maximum difference be-
erical ($M = 96$) and the exact solutions as defined in (56)
$\cdot 10^{-12}$.

ι of the nonstationary equations

ɔroximation of system (42), (43) we use a Galerkin-type
ı method based on Fourier expansion of the prognostic
a finite truncation number M. The system is thus reduced
ıary differential equations for $4M + 2$ Fourier coefficients
$\cdot M \leq k \leq M$:

$$= E_k(\eta_{-M}, \eta_{-M-1}, ..., \eta_M, \phi_{-M}, \phi_{-M-1}, ..., \phi_M) \tag{71}$$

$$= F_k(\eta_{-M}, \eta_{-M-1}, ..., \eta_M, \phi_{-M}, \phi_{-M-1}, ..., \phi_M) \tag{72}$$

where E_k, F_k are, respect
right-hand sides of eqns (

To calculate E_k, F_k as
mulae (23)–(28) are used
uated exactly), and the
transform method (Orsz
evaluation on a spatial gr
tion of its arguments whi
gridpoint values $u(\xi^{(j)})$, v
Fourier transforms are pe
are evaluated at each gr
the function Y are four
$2\pi(j-1)/N$, and N is th

For the method to be
imum mean square appr
need to be evaluated exa
must choose

where ν is the maximum
sides of eqns (42), (43) in
is of infinite order so tha
met. However, numerical
N ensuring exact evaluat
a further increase in N
numerical solution. For n

However high the sp
grations one must paran
of the spectrum ($k > M$
large wavenumbers will c
tion terms were added to
this purpose:

where E_k, F_k are, respectively, the Fourier expansion coefficients for the right-hand sides of eqns (42) and (43) as functions of ξ.

To calculate E_k, F_k as functions of the prognostic variables η_k, ϕ_k, formulae (23)–(28) are used for the spatial derivatives (which are thus evaluated exactly), and the nonlinearities are calculated with the so-called transform method (Orszag, 1970; Eliassen *et al.*, 1970), i.e., by their evaluation on a spatial grid. If $Y(u(\xi), v(\xi), w(\xi), ...)$ is a nonlinear function of its arguments which are represented by their Fourier expansions, gridpoint values $u(\xi^{(j)})$, $v(\xi^{(j)})$, $w(\xi^{(j)})$,... are first calculated, i.e., inverse Fourier transforms are performed; then $Y^{(j)} = Y(u(\xi^{(j)}), v(\xi^{(j)}), w(\xi^{(j)}), ...)$ are evaluated at each gridpoint; finally, the Fourier coefficients Y_k of the function Y are found by direct Fourier transform. Here $\xi^{(j)} = 2\pi(j-1)/N$, and N is the number of gridpoints.

For the method to be a purely Galerkin one, i.e., to ensure the minimum mean square approximation error, the Fourier coefficients E_k, F_k need to be evaluated exactly for $-M \le k \le M$. For this purpose, we must choose

$$N > (\nu + 1)M \qquad (73)$$

where ν is the maximum order of nonlinearities. Since the right-hand sides of eqns (42), (43) include division by the Jacobian, the nonlinearity is of infinite order so that, strictly, the above condition on N cannot be met. However, numerical integrations show that if we choose a value of N ensuring exact evaluation of the cubic nonlinearities ($\nu = 3$ in (73)), a further increase in N (with fixed M) virtually does not impact the numerical solution. For most runs, $M = 96$ and $N = 432$ were used.

However high the spectral resolution might be, for long-term integrations one must parameterize the energy flux into the severed part of the spectrum ($k > M$); otherwise, spurious energy accumulation at large wavenumbers will corrupt the numerical solution. Simple dissipation terms were added to the right-hand sides of eqns (71) and (72) for this purpose:

$$\dot{\eta}_k = E_k - \mu_k \eta_k \ , \qquad (74)$$

$$\dot{\phi}_k = F_k - \mu_k \phi_k \ ; \qquad (75)$$

$$\mu_k = \begin{cases} rM\left(\frac{|k|-k_d}{M-k_d}\right)^2 & \text{if } |k| > k_d \\ 0 & \text{otherwise} \end{cases} \tag{76}$$

and $r = 0.25$ were chosen for most runs; the sensi-
ts to reasonable variations of k_d and r was low. The
vely absorbs the energy at wavenumbers close to the
r M while leaving longer waves virtually intact (note
s $-k_d \leq k \leq k_d$ are not affected).

ation, the fourth-order Runge–Kutta scheme was used.

of the model

lutions dealt with in Section 3 were used for validation
ry model (system (42), (43)). In the model's coordinate
the mean flow, progressive waves were simulated start-
nditions calculated as stationary solutions in a moving
ase of the wave) coordinate system. If such a wave is
t to truncation errors, it should propagate with its spe-
y without changes of shape. The model was validated
waves (experiments 1–3 in Table 3, respectively); pure
scribed analytically by (67)–(70) (Crapper, 1957); pure
aves; and gravity-capillary waves obtained numerically
ction 3.

eqns (45), (46) for Crapper's waves ($\alpha = 0$) was per-
ue of $A = 0.7$ up to $\tau = 100$, i.e., for about 16 periods
the time step $\Delta\tau = 0.001$. Stokes waves ($\sigma = 0$)
ary waves ($\sigma = 0.4$) were simulated for $A = 0.3$ up to
$\tau = 0.01$) and $\tau = 100$ (with $\Delta\tau = 0.001$), respectively.
n of instantaneous wave profiles (not shown) obtained
s of τ during the simulations showed that in all cases the
ithout any visible disturbances. To estimate "steadi-
erical solution quantitatively, we calculated the phase
plitudes of the Fourier components for consecutive val-
rvals of $8\Delta\tau$ and obtained their temporal means and
ns over the period of integration (Table 4).

Table 3: List of numerical
waves; GC – gravity-capill
power spectrum (83) with p
of kth Fourier component of
components of the initial cc

No.	*Type*
1	C
2	G
3	$GC, \sigma = 0.4$
4	$GC, \sigma = 0.05$
5	G
6	G
7	G
8	$GC, \sigma = 0.005$
9	C
10	G

The instantaneous p
calculated as follows:

$$C$$

where η_k are the Fourie
by expansion (11), and

$$\eta(\xi, \tau) =$$

If there is only one wa
sponding to wavenumb
face propagates with a
stant value of C for ea
their shapes, this value
there may be many n
nents) which have the
phase speed due to n
waves there are, gener
rections with the same

Table 3: List of numerical experiments (G – pure gravity waves; C – pure capillary waves; GC – gravity-capillary waves; A – amplitude of stationary wave (55); PS – power spectrum (83) with parameters k_0 , A_0 ; RP – random phases; a_k – amplitude of kth Fourier component of surface height. The last column indicates nonzero Fourier components of the initial conditions, in ξ-coordinate)

No.	*Type*	*Initial conditions*	*Modes*
1	C	*Crapper's wave*, $A = 0.7$	*All*
2	G	*Stokes wave*, $A = 0.3$	*All*
3	$GC, \sigma = 0.4$	*Stationary GC wave*, $A = 0.3$	*All*
4	$GC, \sigma = 0.05$	*PS, RP*, $k_0 = 1$, $A_0 = 0.1$	$1 - 25$
5	G	*Lake & Yuen waves*, $a_3 = a_5 = 0.04$	$3, 5$
6	G	*White noise*, $a_k = 0.001$	$1 - 25$
7	G	*PS, RP*, $k_0 = 5$, $A_0 = 0.01$	$1 - 25$
8	$GC, \sigma = 0.005$	*PS, RP*, $k_0 = 5$, $A_0 = 0.01$	$1 - 25$
9	C	*PS, RP*, $k_0 = 5$, $A_0 = 0.01$	$1 - 25$
10	G	*Stokes wave*, $A = 0.3$, + *white noise*, $a_k = 0.001$	*All*+ $15 - 39$

The instantaneous phase velocity of the kth wave component may be calculated as follows:

$$C(k) = \dot{\lambda}_k = \frac{\eta_{-k}\dot{\eta}_k - \eta_k\dot{\eta}_{-k}}{k(\eta_k^2 + \eta_{-k}^2)}, \tag{77}$$

where η_k are the Fourier expansion coefficients of the surface as defined by expansion (11), and λ_k are the phases:

$$\eta(\xi,\tau) = \sum_{0 \le k \le M} \sqrt{\eta_k^2 + \eta_{-k}^2} \cos\left(k(\xi - \lambda_k(\tau))\right).$$

If there is only one wavenumber–frequency spectrum component corresponding to wavenumber k, i.e., if each Fourier component of the surface propagates with a single phase velocity, formula (77) yields a constant value of C for each k. In our case of progressive waves retaining their shapes, this value is the same for all k. For arbitrary wave fields, there may be many modes (wavenumber–frequency spectrum components) which have the same wavenumber but propagate with different phase speed due to nonlinear effects, and even in the case of linear waves there are, generally, two kth modes propagating in opposite directions with the same absolute speed. In such cases, formula (77) yields age phase velocity of the modes, which generally vary in scribed runs, modes moving in the opposite direction were ng the integration because of truncation errors. The am-e modes were by several orders of magnitude smaller than ;rue" (positively directed) components of the simulated manifest themselves in small shifts and perturbations of ›us phase velocities, whose temporal means and standard given in Table 4 for the first 15 modes.

al means and standard deviations of the phase velocities for the Crapper's, Stokes and gravity-capillary progressive waves (C is the ›city, i.e. that obtained for the stationary solution)

waves	*Stokes waves*	*GC waves*
).971524	$A = 0.3,\ C = 1.046040$	$A = 0.3,\ C = 1.160514$
$1 \cdot 10^{-5})$	$1.045997\ (2 \cdot 10^{-5})$	$1.160514\ (2 \cdot 10^{-5})$
$1 \cdot 10^{-5})$	$1.045940\ (2 \cdot 10^{-5})$	$1.160513\ (2 \cdot 10^{-5})$
$1 \cdot 10^{-5})$	$1.045844\ (2 \cdot 10^{-5})$	$1.160512\ (2 \cdot 10^{-5})$
$1 \cdot 10^{-5})$	$1.045711\ (2 \cdot 10^{-5})$	$1.160510\ (2 \cdot 10^{-5})$
$1 \cdot 10^{-5})$	$1.045539\ (2 \cdot 10^{-5})$	$1.160507\ (2 \cdot 10^{-5})$
$1 \cdot 10^{-5})$	$1.045329\ (2 \cdot 10^{-5})$	$1.160505\ (2 \cdot 10^{-5})$
$1 \cdot 10^{-5})$	$1.045081\ (2 \cdot 10^{-5})$	$1.160501\ (2 \cdot 10^{-5})$
$1 \cdot 10^{-5})$	$1.044790\ (2 \cdot 10^{-5})$	$1.160497\ (2 \cdot 10^{-5})$
$1 \cdot 10^{-5})$	$1.044472\ (2 \cdot 10^{-5})$	$1.160493\ (2 \cdot 10^{-5})$
$\cdot 10^{-5})$	$1.044410\ (2 \cdot 10^{-5})$	$1.160488\ (2 \cdot 10^{-5})$
$\cdot 10^{-5})$	$1.043709\ (2 \cdot 10^{-5})$	$1.160482\ (2 \cdot 10^{-5})$
$\cdot 10^{-5})$	$1.043271\ (2 \cdot 10^{-5})$	$1.160476\ (2 \cdot 10^{-5})$
$\cdot 10^{-5})$	$1.042795\ (2 \cdot 10^{-5})$	$1.160470\ (2 \cdot 10^{-5})$
$\cdot 10^{-5})$	$1.042281\ (2 \cdot 10^{-5})$	$1.160463\ (2 \cdot 10^{-5})$
$\cdot 10^{-4})$	$1.041730\ (2 \cdot 10^{-5})$	$1.160456\ (2 \cdot 10^{-5})$

d phase velocities are very close to their values obtained solutions (also given in Table 4); although they slightly reasing the wavenumber, their mean errors and standard nall for all the three types of waves. Since conservation s (not shown) was also very accurate (the deviations of ng the simulations from their initial values were always r the Stokes wave and less than 10^{-11} for the capillary

and gravity-capillar and remained consis not noticeably chan implies that these wa that the numerical s tions of the original

Another criterion invariants during the

horizontal momentu

and energy $E = E_K$

is the kinetic energy,

is the potential energ

E

is the potential ener tained by transform for the invariants int the horizontal axis.

An example of th resented in Fig. 5 fo The initial surface wa linear modes with an

$a_k = \langle$

which generally vary in
opposite direction were
cation errors. The am-
magnitude smaller than
nents of the simulated
ts and perturbations of
al means and standard
odes.

ne phase velocities for the
progressive waves (C is the
y solution)

GC waves
$A = 0.3,\ C = 1.160514$
1.160514 $(2 \cdot 10^{-5})$
1.160513 $(2 \cdot 10^{-5})$
1.160512 $(2 \cdot 10^{-5})$
1.160510 $(2 \cdot 10^{-5})$
1.160507 $(2 \cdot 10^{-5})$
1.160505 $(2 \cdot 10^{-5})$
1.160501 $(2 \cdot 10^{-5})$
1.160497 $(2 \cdot 10^{-5})$
1.160493 $(2 \cdot 10^{-5})$
1.160488 $(2 \cdot 10^{-5})$
1.160482 $(2 \cdot 10^{-5})$
1.160476 $(2 \cdot 10^{-5})$
1.160470 $(2 \cdot 10^{-5})$
1.160463 $(2 \cdot 10^{-5})$
1.160456 $(2 \cdot 10^{-5})$

their values obtained
lthough they slightly
n errors and standard
s. Since conservation
te (the deviations of
l values were always
$^{-11}$ for the capillary

and gravity-capillary waves), the modes retained their initial energies and remained consistent in phase; consequently, the simulated waves did not noticeably change their shapes during the integration. This result implies that these waves are stable with respect to truncation errors, and that the numerical solutions yielded by the model approximate the solutions of the original differential equations with high accuracy.

Another criterion of model accuracy is conservation of the integral invariants during the integration, i.e. of volume

$$V = (2\pi)^{-1} \int_0^{2\pi} z x_\xi \mathrm{d}\xi, \tag{78}$$

horizontal momentum

$$I = (2\pi)^{-1} \int_0^{2\pi} \phi z_\xi \mathrm{d}\xi, \tag{79}$$

and energy $E = E_K + E_{PG} + E_{PT}$, where

$$E_K = (2\pi)^{-1} \int_0^{2\pi} \phi \phi_\zeta \mathrm{d}\xi \tag{80}$$

is the kinetic energy,

$$E_{PG} = (2\pi)^{-1} \int_0^{2\pi} z^2 x_\xi \mathrm{d}\xi \tag{81}$$

is the potential energy of gravity, and

$$E_{PT} = (2\pi)^{-1} \sigma \int_0^{2\pi} (J^{-1/2} - 1) \mathrm{d}\xi \tag{82}$$

is the potential energy of surface tension. Formulae (78)–(82) are obtained by transformation of standard Cartesian-coordinate expressions for the invariants into (ξ, ζ) coordinates and refer to a unit length along the horizontal axis.

An example of the temporal evolution of E_K, E_P, E_T, and E is represented in Fig. 5 for the case of gravity-capillary waves with $\sigma = 0.05$. The initial surface was chosen in the form of a superposition of $M_m = 25$ linear modes with amplitudes a_k assigned according to

$$a_k = \begin{cases} A_0 \left(\frac{k}{k_0}\right)^P & k_0 \le k \le k_0 + M_m - 1 \\ 0 & \text{otherwise} \end{cases} \tag{83}$$

ıplitude of the k_0th mode, and power $P < 0$ is The Fourier coefficients were calculated as

$$= a_k \begin{cases} \sin \lambda_k & k \leq 0 \\ \cos \lambda_k & k > 0 \end{cases} \quad (84)$$

phases.

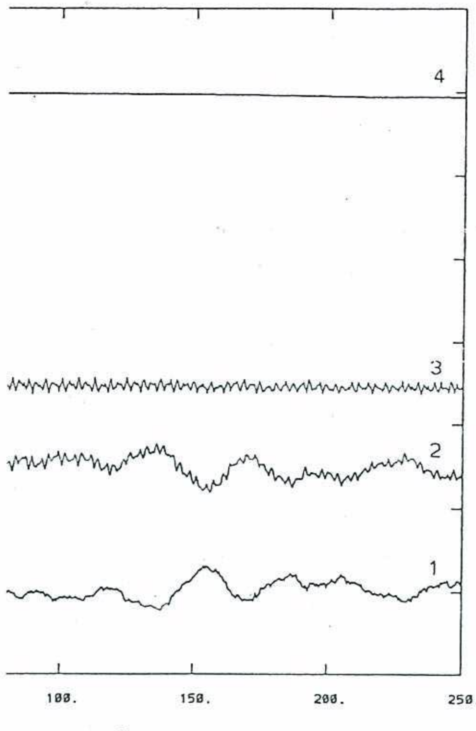

ɔtential energy of surface tension E_{PT} (curve 1), gravi- (2), kinetic energy E_K (3), and their sum E (4) (Exp. ($\sigma = 0.05$).

ɜ for the initial surface velocity potential Φ were r approximation, all wave components propa- ction. It can be easily derived from the linear

theory that this is ensured by

$$\phi_k = b_k \eta_{-k}, \quad b,$$

For the calculations repre $P = -\frac{3}{2}$, $k_0 = 1$, $M_m = 25$, tal momentum I and the volu margins of the order of 10^{-13} can be seen that while the ene significant fluctuations, their due to damping at high waven a number of other test simulat

The results described in th cessfully simulate evolution of

6. Results of the simu

The progressive gravity, capill in Sections 3 and 5 represent a they consist of Fourier modes sion relation (59), propagate evident that similar effects ma tions: due to the impact of no not be represented as a superp their linear phase speeds; mor not associated with any single manifestation of nonlinearity i phase speeds close to that of lo "bound") components was cle observational studies (Yuen an been proposed for this phen current coupling, but Lake a mainly due to nonlinearity of contain both types of waves, f and the "observed" phase velo Partitioning of the energy bet wave spectrum, whose shape oretical explanation of this e

th mode, and power $P < 0$ is
fficients were calculated as

$$\leq 0$$
$$> 0 \qquad (84)$$

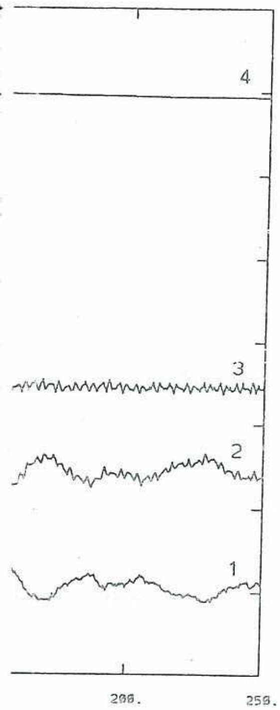

ace tension E_{PT} (curve 1), gravi-
$_K$ (3), and their sum E (4) (Exp.

ace velocity potential Φ were
all wave components propa-
asily derived from the linear

theory that this is ensured by the relations:

$$\phi_k = b_k \eta_{-k}, \quad b_k = \mathrm{sign}(k)\sqrt{\frac{1+\sigma k^2}{k\tanh(kH)}}. \qquad (85)$$

For the calculations represented in Fig. 5, $\sigma = 0.05$, $A_0 = 0.1$, $P = -\frac{3}{2}$, $k_0 = 1$, $M_m = 25$, and $H = \infty$ (deep water). The horizontal momentum I and the volume V were conserved with relative error margins of the order of 10^{-13} and 10^{-11} respectively. From Fig. 5 it can be seen that while the energy components E_K, E_{PG}, and E_{PT} show significant fluctuations, their sum nearly conserves; its slow decrease is due to damping at high wavenumbers. Similar results were obtained for a number of other test simulations, including ones with a finite depth H.

The results described in this section suggest that the model can successfully simulate evolution of multi-component wave fields.

6. Results of the simulations

The progressive gravity, capillary, and gravity-capillary waves dealt with in Sections 3 and 5 represent a very special case of nonlinear interactions; they consist of Fourier modes which, rather than obey the linear dispersion relation (59), propagate with one and the same phase speed. It is evident that similar effects may also be observed in more general situations: due to the impact of nonlinearity, a multi-mode wave motion cannot be represented as a superposition of Fourier modes propagating with their linear phase speeds; moreover, a specific wavenumber, generally, is not associated with any single phase speed. Perhaps the most striking manifestation of nonlinearity is that some shorter waves propagate with phase speeds close to that of long waves. The existence of such forced (or "bound") components was clearly demonstrated in many laboratory and observational studies (Yuen and Lake, 1982). Various explanations have been proposed for this phenomenon, including wind–wave and wave–current coupling, but Lake and Yuen (1978) found that this effect is mainly due to nonlinearity of the waves themselves. Realistic wave fields contain both types of waves, free and bound, for the same wavenumber, and the "observed" phase velocities reflect a combined effect of the two. Partitioning of the energy between these types of waves depends on the wave spectrum, whose shape is influenced by external forcing. A theoretical explanation of this effect based on Zakharov's (1968) equation

Yuen and Lake (1982). The phenomenon was repro-
·drodynamical potential wave model by Chalikov and
vho pointed out that, with phase velocities calculated
ula (77), each Fourier component turns out to have a
much greater than that predicted by the linear theory.
ıat the phase velocity varies in time, and that its stan-
:reases with the wavenumber. However, their model
long-term simulations with high spectral resolution,
eater computational efficiency and accuracy. Experi-
model described above has shown that, for analysis
equency spectra to be virtually unaffected by further
del resolution and the length of simulations, it is es-
odel be run for several hundred periods of the longest
:tral truncation number M of the order of 100. In the
ow, $M = 96$ and $N = 432$ were used.

nsider the results of a model simulation (Exp. 5) of
ıents by Lake and Yuen (1978) who investigated the
on of two gravity waves with wavenumbers close to
evaluated the phase velocities of different modes by
erence of the surface elevation values in two sections
(Fig. 8 of Lake and Yuen, 1978), and found out that
s of the waves not produced by the wave maker were
e primary waves. It is hardly possible to exactly re-
:iment in a model simulation, since the amplitudes of
reported, and there are uncertainties as to modeling
the model, to obtain a flow qualitatively similar to
ment, we used a superposition of the 3rd and the 5th
nplitudes of 0.04 as the initial conditions for the sur-
rcing was imposed. In this and all other runs (except
progressive waves described in Section 3), the initial
velocity potential on the surface were prescribed ac-
r theory for unidirectional waves (formula (85)). The
ormed with $\Delta\tau = 0.01$ up to $\tau = 1000$.

r spectra (calculated from Fourier expansions of the
ith respect to x coordinate) averaged for 6 consec-
(167 nondimensional time units each) are given in
y decreases slowly in time because of dissipation at

high wavenumbers. Th
the energy of the 5th m
mode) is considerably l

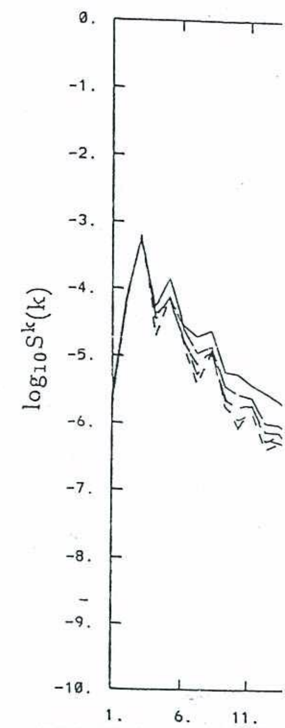

Figure 6: Time-averaged wa
of length $\delta\tau = 167$, Exp. 5.

In Fig. 7, temporal
neous phase velocities (7
relation is observed only
waves propagate significa
the primary waves. This
ral means of the phase ve
pointed out in Chalikov
standard deviations for
by the presence of both

high wavenumbers. The energy of the 3rd mode is nearly conserved but the energy of the 5th mode (which was initially equal to that of the 3rd mode) is considerably less.

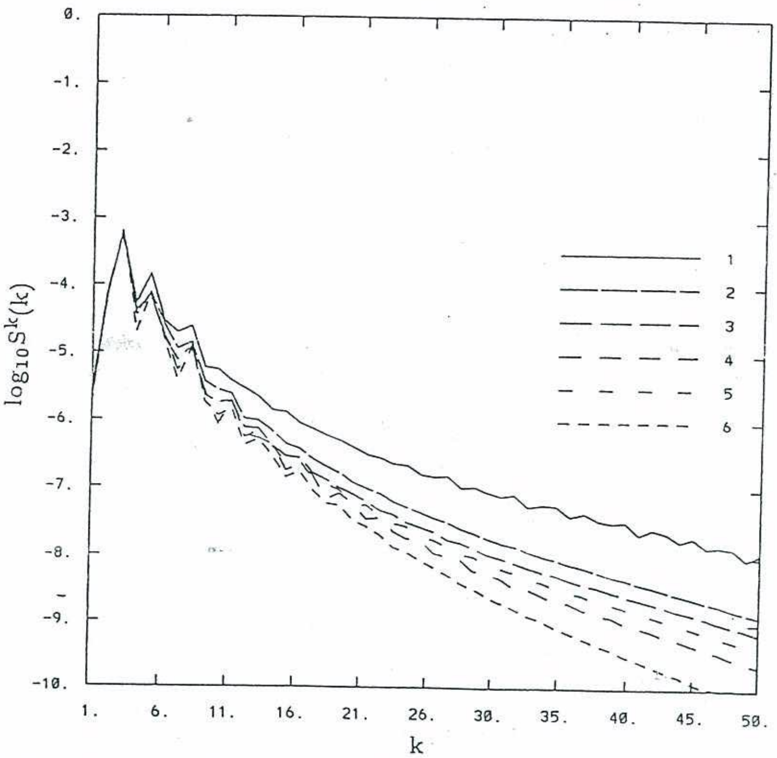

Figure 6: Time-averaged wavenumber spectra $S^k(k)$ for 6 consecutive time intervals of length $\delta\tau = 167$, Exp. 5.

In Fig. 7, temporal means and standard deviations of the instantaneous phase velocities (77) are shown. It is seen that the linear dispersion relation is observed only for wavenumbers $2 \leq k \leq 5$. For $k > 5$, the waves propagate significantly faster than the linear waves but slower than the primary waves. This effect is clearly pronounced only for the temporal means of the phase velocities; the instantaneous values vary highly (as pointed out in Chalikov and Liberman, 1991), which is reflected by large standard deviations for wavenumbers $k > 5$. This scattering is caused by the presence of both bound and free waves.

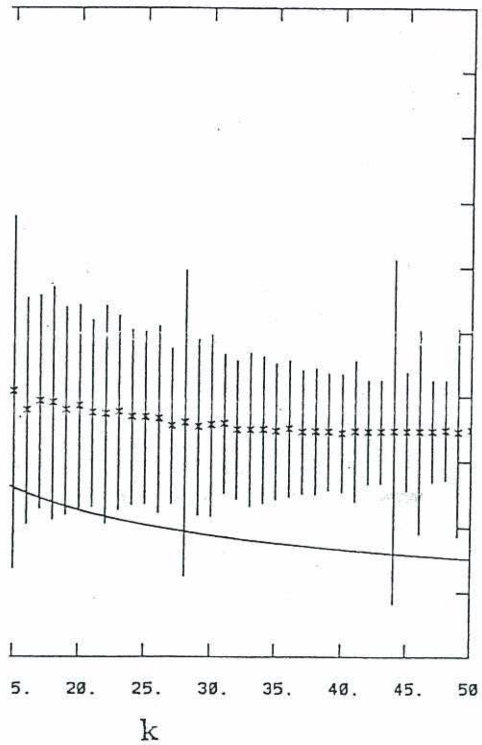

e velocity (77) (∗) and its standard deviation (vertical
ıber k, Exp. 5 (simulation of the nonwind experiment
ɜ curve corresponds to the linear dispersion relation.

free and bound waves and their phase veloci-
avenumber–frequency spectrum $S(k,\omega)$ whose
g. 8 along with the logarithms of the time-
$^{c}(k)$) and frequency ($S^{\omega}(\omega)$) spectra. The pic-
nsisted of patches; this effect is caused by the
ur lines. To calculate S for each k, instanta-
with respect to the x coordinate were stored
ıf integration $0 \le \tau \le 1000$ with time intervals
ıforms with respect to time were used. In this
ı of simulation ensured sufficient frequency res-
000), which is essential for the analysis of the

spectra, and the maximum res
far exceeded any possible "ph
transforms' aliasing error negli

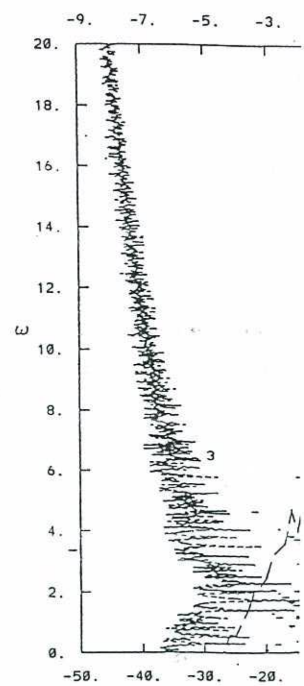

Figure 8: Time-averaged spectral
5. Curve 1 – linear dispersion relat
1, 2, ..., 9. The contour lines of log
seen as concatenated in patches. Cu
scale), Curve 3 is $\log_{10} S^{\omega}(\omega)$ (frequ

The most remarkable featu
is that it is split into a set of
well pronounced for the wave
originally by using relations
ticeable for the waves moving
present in the initial conditio
is determined by the sign of

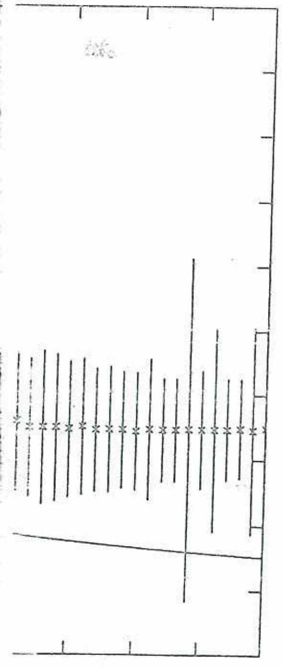

spectra, and the maximum resolved frequency ($\omega = \pi/0.08$ for this run) far exceeded any possible "physical" value of ω and thus rendered the transforms' aliasing error negligible.

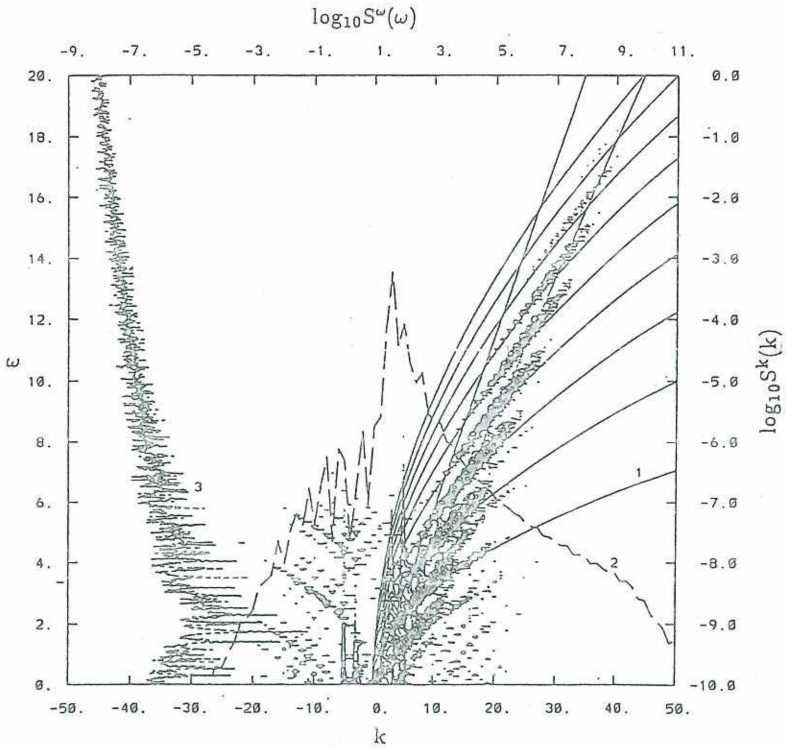

Figure 8: Time-averaged spectral characteristics for the period of $\delta\tau = 1000$, Exp. 5. Curve 1 – linear dispersion relation $\omega^2 = k$, the other parabolas – $\omega^2 = nk$, $k = 1, 2, \ldots, 9$. The contour lines of $\log_{10} S(k,\omega)$ (wavenumber–frequency spectrum) are seen as concatenated in patches. Curve 2 is $\log_{10} S^k(k)$ (wavenumber spectrum, right scale), Curve 3 is $\log_{10} S^{\omega}(\omega)$ (frequency spectrum, top scale).

The most remarkable feature of the wavenumber–frequency spectrum is that it is split into a set of branches in a regular way. This effect is well pronounced for the waves propagating in the direction prescribed originally by using relations (85) ($k > 0$ in Fig. 8), but it is also noticeable for the waves moving in the opposite direction, which were not present in the initial conditions ($k < 0$ in Fig. 8 where the sign of k is determined by the sign of the component's phase velocity, while ω is

\ considerable part of energy is borne by the compo-
ɔbey the linear dispersion relation $\omega^2 =| k |$ (Curve
ɛnergy mostly belongs to what may be, with some
ɔreted as bound components, which propagate with
ɔf their carrying waves from near Curve 1 and lie on
imated by the curves

$$\omega^2 = n \mid k \mid, \tag{86}$$

r of the branch) is a positive integer. (Strictly, not
s (86) with $n > 1$ may be called bound, since those
a multiple of n have no "carrier". However, they
were bound to a free wave with wavenumber k/n).

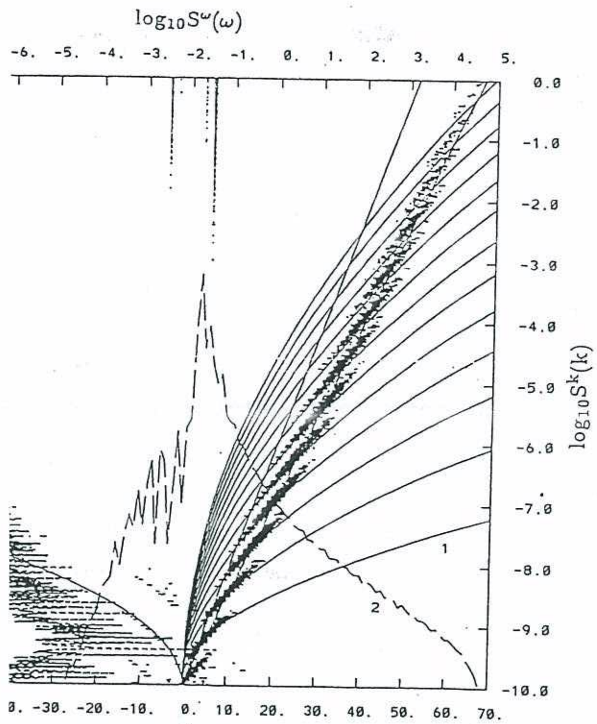

. 8, but instead of $\log_{10} S$ the contours of normalized spec-
ɔlotted.

Each of the branches
bers k and tends to stra
increasing, the group vel
is the same for all the b
are also other patterns w
notably regular discrete

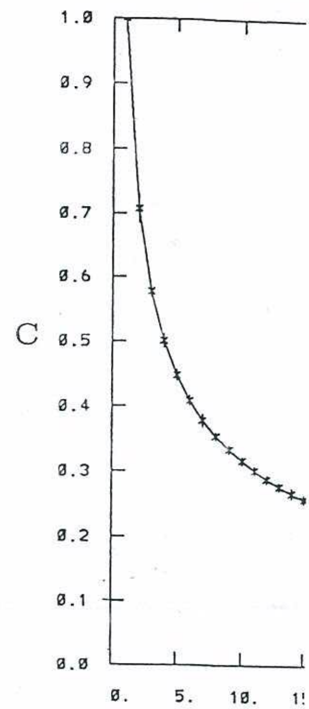

Figure 10: Same as in Fig. 7
noise).

Another representatio
be obtained through norı
for a given k is the spect
spectrum (Fig. 9), which
over frequencies for each
type described above. A

:t of energy is borne by the compo-
spersion relation $\omega^2 = | k |$ (Curve
longs to what may be, with some
components, which propagate with
waves from near Curve 1 and lie on
rves

$$k |, \tag{86}$$

s a positive integer. (Strictly, not
may be called bound, since those
ave no "carrier". However, they
rce wave with wavenumber k/n).

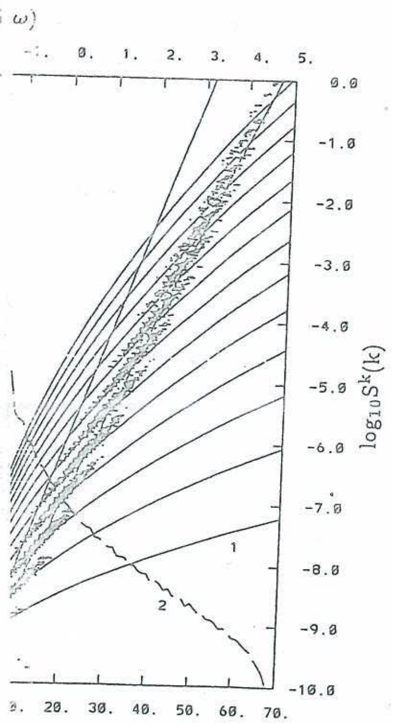

$_{10} S$ the contours of normalized spec-

Each of the branches follows relation (86) closely at lower wavenumbers k and tends to straighten at higher wavenumbers so that, with k increasing, the group velocity appears to tend to a constant whose value is the same for all the branches. Along with this set of branches, there are also other patterns which, despite their relatively low energy, show a notably regular discrete structure.

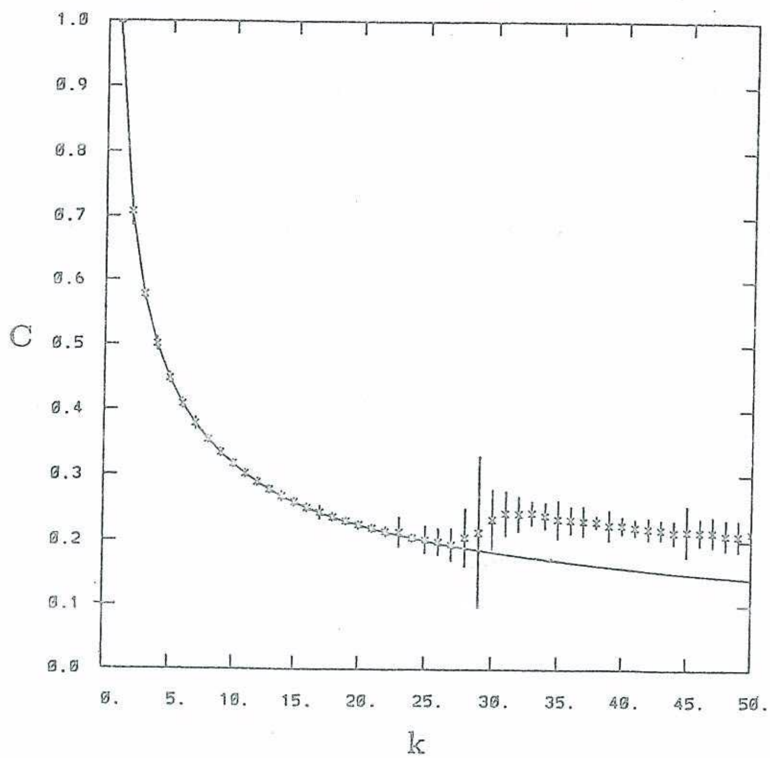

Figure 10: Same as in Fig. 7 but for Exp. 6 (initial conditions approximating white noise).

Another representation of the wavenumber–frequency spectrum can be obtained through normalizing each value of $S(k,\omega)$ by $S^k(k)$ (which for a given k is the spectral density integrated over ω). The normalized spectrum (Fig. 9), which characterizes the fractional energy distribution over frequencies for each wavenumber, exhibits up to 13 branches of the type described above. A most peculiar feature of the spectrum, clearly

), is a pattern which may be approximated by
rough the origin of the coordinates; the corre-
.d to propagate with roughly the same phase
)e equal to the aforementioned apparent limit

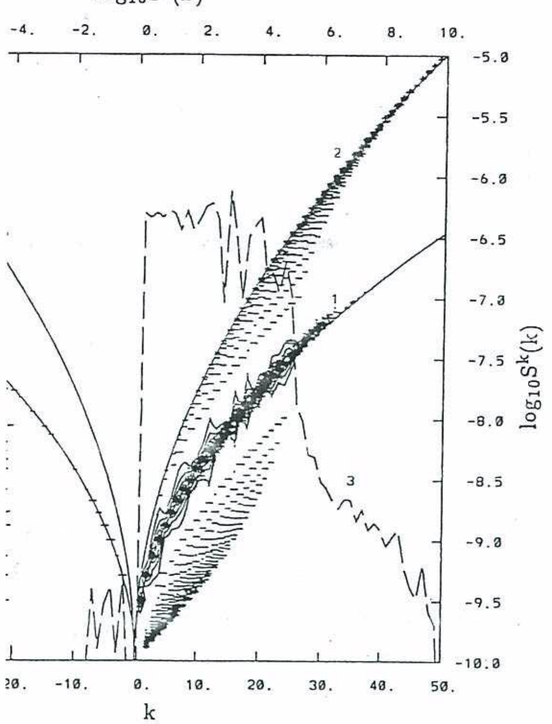

acteristics as in Fig. 8 but for "white noise" simulation
dispersion relation $\omega^2 = nk$ ($n = 1,\ 2$), 3 – $S^k(k)$, 4 –

xperiment (Exp. 6) simulated a pure gravity
iditions approximating white noise; other fea-
ı Exp. 5. For the first 25 wavenumbers k, the
ssigned the same value of 0.001, with random
mplitudes were set to zero. The phase veloci-
ırd deviations are shown in Fig. 10. Because

the amplitudes of the initia
nearly obey the linear theor
ear ones and have small sta
the nonlinear interactions (
waves. In the wavenumber–
two ($n = 1$, where most of t
"main branches" approxima
the energy is small, and, aga
line passing through the orig
other regularly located curv
planation of these features.

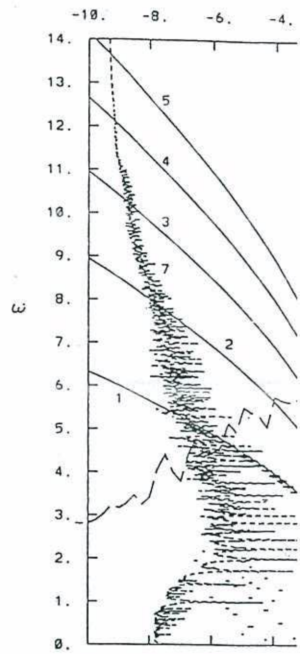

Figure 12: Same spectral charact
with spectrum (83) approximatir

Another run (Exp. 7),

which may be approximated by
ı of the coordinates; the corre-
with roughly the same phase
aforementioned apparent limit

)

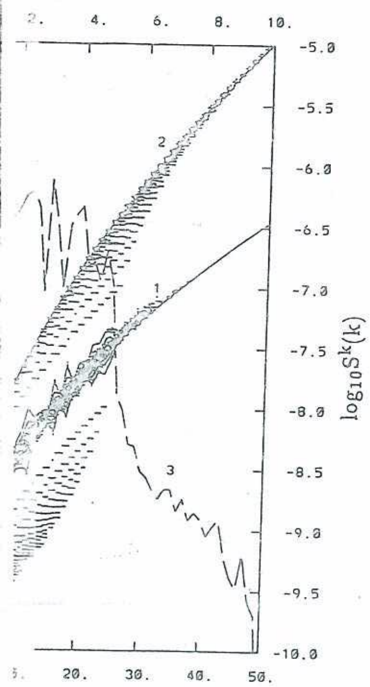

8 but for "white noise" simulation
$\omega^2 = nk$ ($n = 1, 2$), 3 – $S^k(k)$, 4 –

6) simulated a pure gravity
nating white noise; other fea-
first 25 wavenumbers k, the
value of 0.001, with random
en to zero. The phase veloci-
shown in Fig. 10. Because

the amplitudes of the initially assigned waves were small, these waves nearly obey the linear theory: their phase velocities are close to the linear ones and have small standard deviations. The waves produced by the nonlinear interactions ($k > 25$) again propagate faster than linear waves. In the wavenumber–frequency spectrum (Fig. 11), only the first two ($n = 1$, where most of the energy is concentrated, and $n = 2$) of the "main branches" approximated by (86) are seen. The remaining part of the energy is small, and, again, most of it is concentrated near a straight line passing through the origin, while the remainder is distributed along other regularly located curves. Further investigations are needed for explanation of these features.

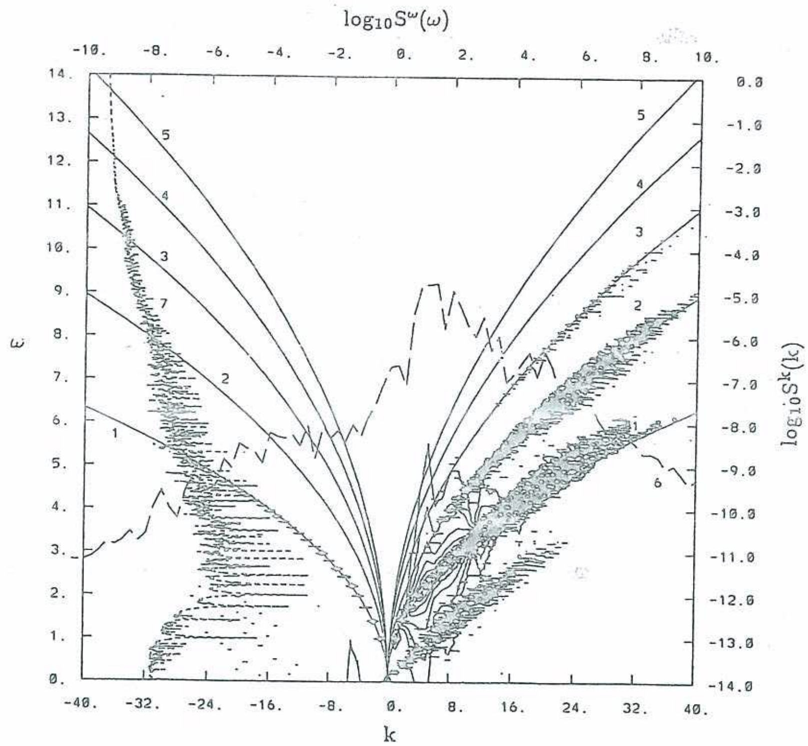

Figure 12: Same spectral characteristics as in Fig. 8 but for Exp. 7 (initial conditions with spectrum (83) approximating real waves).

Another run (Exp. 7), which also differed from the previously de-

ımplitudes only, was designed to approximate
e initial spectrum of the surface elevation was
ł), with $A_0 = 0.01$, $k_0 = 5$, $P = -1.5$. The
12. In the wavenumber–frequency spectrum,
.ergy concentrated along the "main" branches
near" branch is again quite distinct.

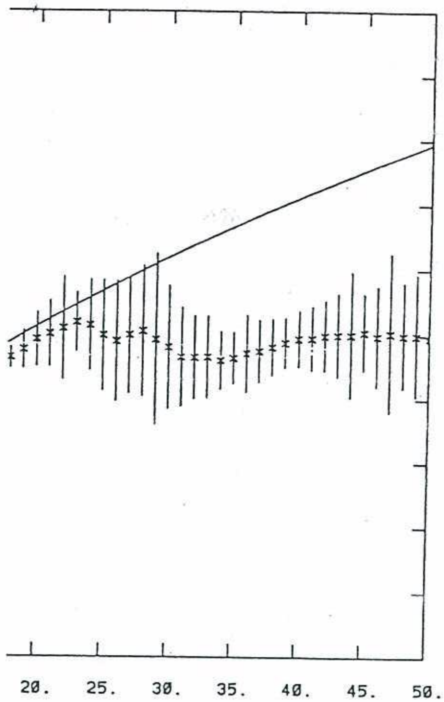

for Exp. 8 (gravity-capillary waves, $\sigma = 0.005$).

gravity-capillary waves were simulated, with
ity coefficient $\sigma = 0.005$. The initial condi-
; to (83) and (84) with $A_0 = 0.01$, $k_0 = 5$,
'aves bearing most of the energy the gravity
f the same order. The time integration was
with the time step $\Delta\tau = 0.01$. The depen-
and its temporal standard deviation on the

wavenumber is shown in Fig. 13.

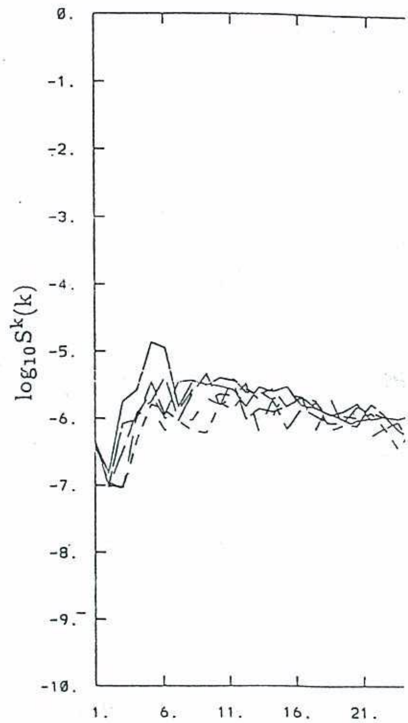

Figure 14: Same as Fig. 6 but for Exp.

As in the runs with pure gravi
to follow the linear dispersion re
scattering, while the shorter wave
nonlinear interactions, tend to a
characteristic for longer waves and
by the linear theory. The wavenur
tion is shown in Fig. 14 in the s
whose mean over the period of in
Fig. 15, shows a greater nonline
than in the case of pure gravity
less steep slope of the curve, com
the previous run (Fig. 12, Curve 6

'y, was designed to approximate
'um of the surface elevation was
0.01, $k_0 = 5$, $P = -1.5$. The
venumber–frequency spectrum,
ated along the "main" branches
s again quite distinct.

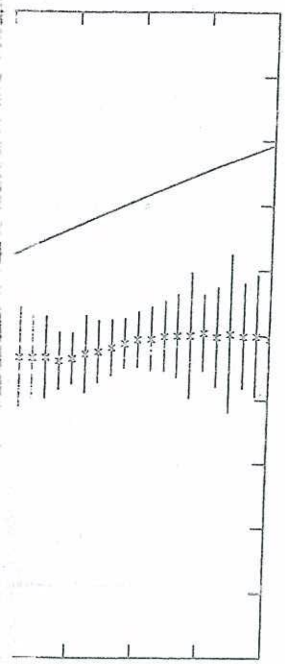

ity-capillary waves, $\sigma = 0.005$).

ry waves were simulated, with
$r = 0.005$. The initial condi-
34) with $A_0 = 0.01$, $k_0 = 5$,
ost of the energy the gravity
er. The time integration was
step $\Delta\tau = 0.01$. The depen-
al standard deviation on the

wavenumber is shown in Fig. 13.

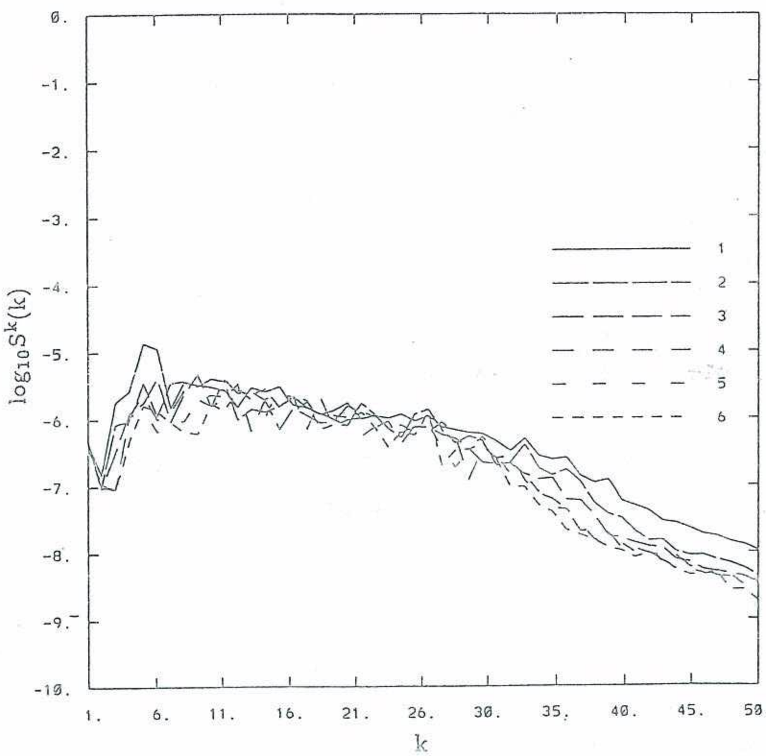

Figure 14: Same as Fig. 6 but for Exp. 8.

As in the runs with pure gravity waves, the lower wavenumbers tend to follow the linear dispersion relation (77), though with considerable scattering, while the shorter waves, which are mostly generated by the nonlinear interactions, tend to assume the phase velocities which are characteristic for longer waves and are in this case lower than those given by the linear theory. The wavenumber spectrum, whose temporal evolution is shown in Fig. 14 in the same way as in Fig. 6 for Exp. 5 and whose mean over the period of integration is represented by Curve 2 in Fig. 15, shows a greater nonlinear energy flux to higher wavenumbers than in the case of pure gravity waves. This is manifested in a much less steep slope of the curve, compared to the corresponding results of the previous run (Fig. 12, Curve 6), which was performed with the same

, and in a relatively fast decrease of energy with on high wavenumbers. The same observation can ncy spectra (compare Fig. 15, Curve 3 and Fig.

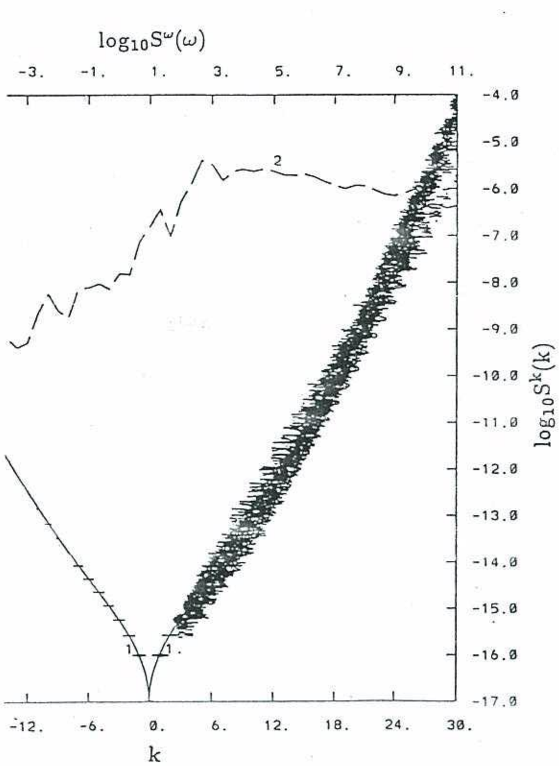

haracteristics as in Fig. 8 but for Exp. 8. Curve 1 – linear in relation (87)), 2 – $\log_{10} S^k(k)$; 3 – $\log_{10} S(k,\omega)$.

equency spectrum (Fig. 15), it is hard to distin- free and bound waves, since Curve 1 which cor- dispersion relation (59) is too close to a straight gest waves whose energy is negligibly small. Here, d regarding that a bound wave propagates with y ω/k as its carrying wave and has a wavenumber multiple of the latter, we can write the following "main branches":

$$\left(\frac{\omega}{n}\right)^2$$

where $n = 1$ for the free (ca waves. However, the branch

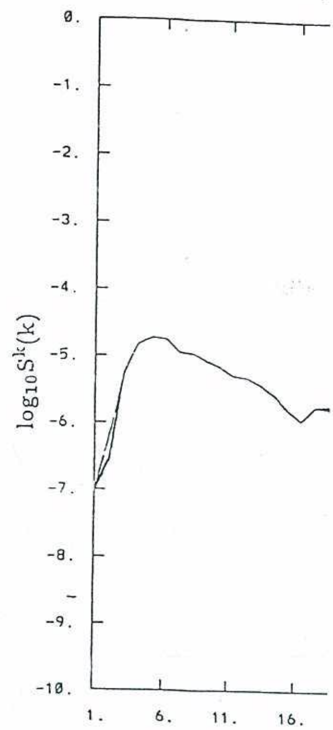

Figure 16: Same as in Fig. 6 but

Results of simulation of (46)) are shown in Figs 16 a in Figs 14 and 15 respective were the same as in Exps 7 a and the time step $\Delta\tau = 0.0$ wavenumber spectrum is mu waves (Exp. 7) than to that wavenumber–frequency spect

$$\left(\frac{\omega}{n}\right)^2 = \frac{|\,k\,|}{n} + \sigma\left(\frac{|\,k\,|}{n}\right)^3, \tag{87}$$

where $n = 1$ for the free (carrying) waves and $n = 2, 3, \ldots$ for the bound waves. However, the branches appear to merge with each other.

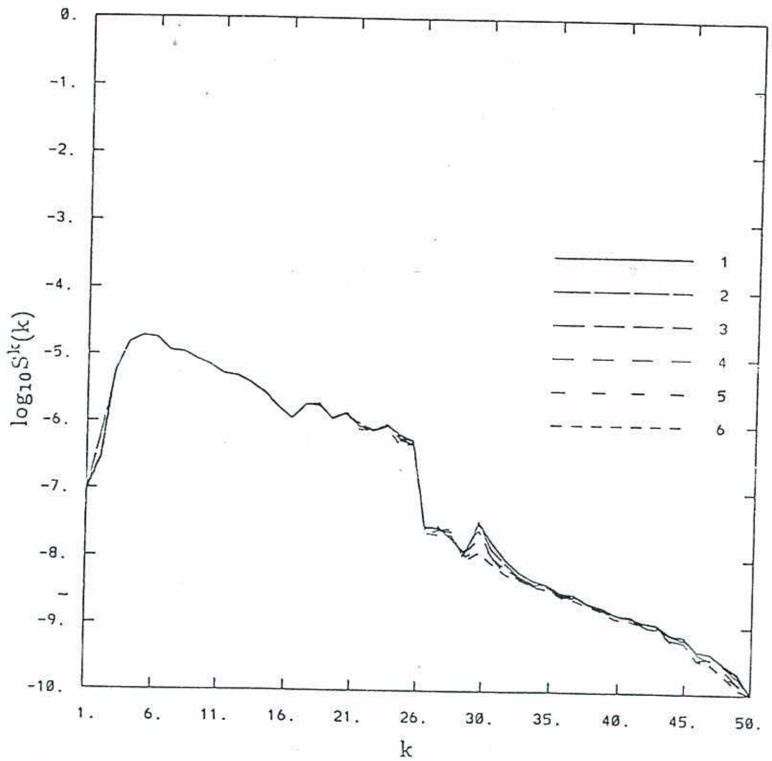

Figure 16: Same as in Fig. 6 but for Exp. 9 (capillary waves), $\delta\tau = 16.7$.

Results of simulation of pure capillary waves (Exp. 9, $\alpha = 0$ in eqn (46)) are shown in Figs 16 and 17 (the same spectral characteristics as in Figs 14 and 15 respectively). The initial values of surface elevation were the same as in Exps 7 and 8; the period of integration was $\tau = 100$, and the time step $\Delta\tau = 0.001$. It is remarkable that the slope of the wavenumber spectrum is much closer to that obtained for pure gravity waves (Exp. 7) than to that of gravity-capillary waves (Exp. 8). The wavenumber–frequency spectrum agrees well with the linear dispersion

Curve 1); however, below the curve is what appears ıain branches" corresponding to bound waves and

$$\omega^2 = \frac{| k |^3}{n} \tag{88}$$

ing from (87) with the gravity term omitted and ; an additional set of waves above the curve which i-rectilinear" patterns observed in the pure gravity es 8, 9, 11, 12 and 17 may suggest the hypothesis :orrespond to waves which, through nonlinear inter- d shorter waves, are forced to propagate with the .e latter; further extensive simulations are needed to 3.

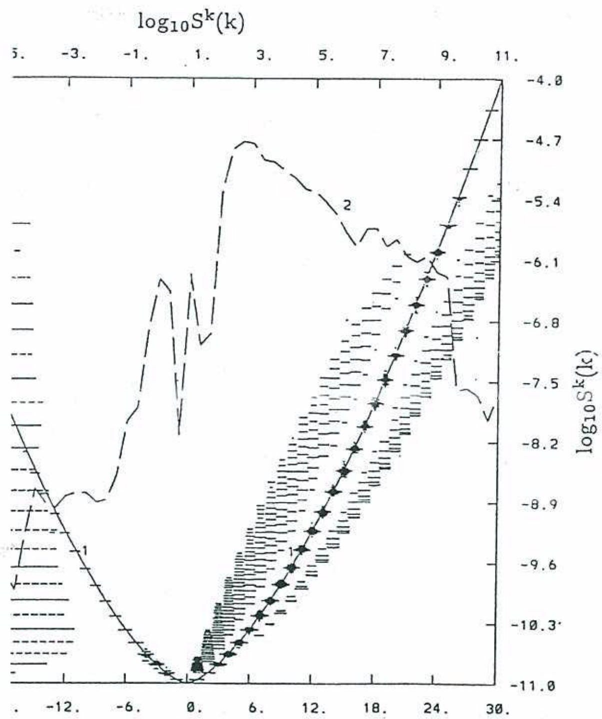

'ig. 8 but for Exp. 9 (capillary waves), with Curve 1 being ıtion ($n = 1$ in relation (88))

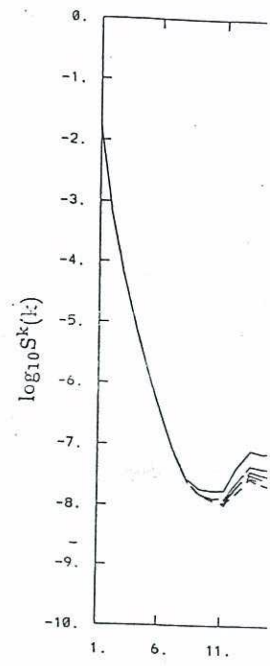

Figure 18: Same as in Fig. (superimposed short gravity w

Besides the simulatic experiments with differen and dissipation paramet external forcing (not disc tra observed in all runs h follows. Most of the ener called "main branches" a bound ($n = 2, 3, \ldots$) wave

and, for not too large k, pure capillary waves).

the curve is what appears
ding to bound waves and

(88)

gravity term omitted and
ves above the curve which
served in the pure gravity
ay suggest the hypothesis
h, through nonlinear inter-
ed to propagate with the
simulations are needed to

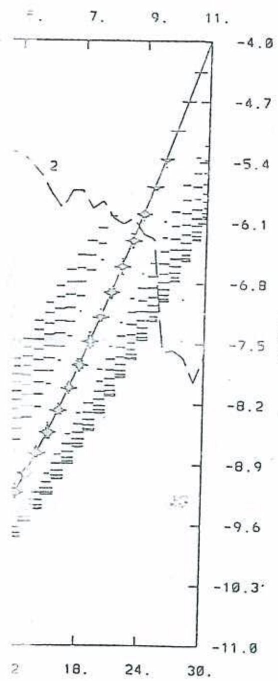

y waves), with Curve 1 being

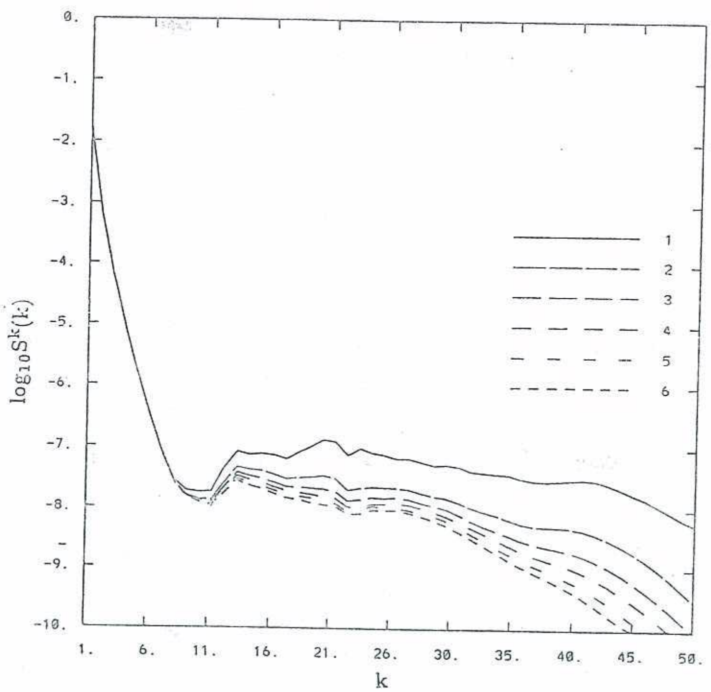

Figure 18: Same as in Fig. 6 but for Exp. 10 (initial conditions: Stokes wave with superimposed short gravity waves).

Besides the simulations described above, we ran a number of other experiments with different initial conditions, resolution in the horizontal, and dissipation parameters; some of the runs included various types of external forcing (not discussed here). The wavenumber–frequency spectra observed in all runs had similar features which may be summarized as follows. Most of the energy is concentrated along the curves which were called "main branches" and which consist of free ($n = 1$) and generalized bound ($n = 2, 3, ...$) waves. The general formula for this set of curves is

$$D\left(\frac{\omega}{n}, \frac{k}{n}\right) = 0 \qquad (89)$$

and, for not too large k, is approximated by relation (87) (or (88) for pure capillary waves).

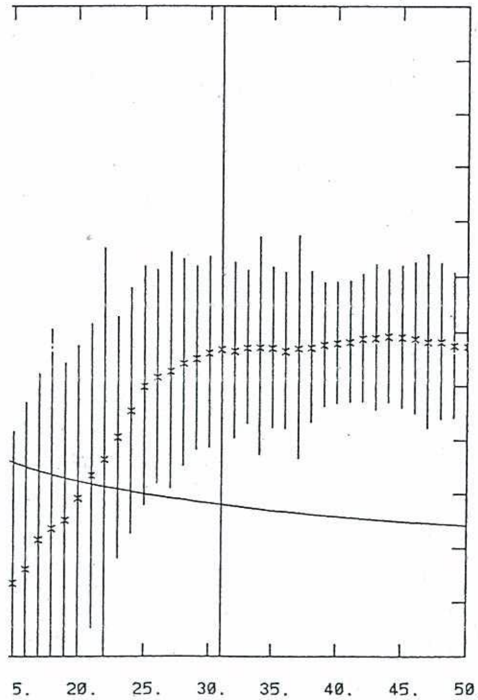

' but for Exp. 10.

ɪn (89), nonlinearity is manifested in two ways: ɪches instead of one curve corresponding to linear ion $D(\omega', k')$ itself differs from its approximation

$$\omega', k') = \omega'^2 - \mid k' \mid - \sigma \mid k' \mid^3 \qquad (90)$$

ɔry. The specific form of D depends on the energy ɔectrum and is determined by external forcing tions. For example, in the very special case of a

$$D(\omega', k') = \omega' - ck' \qquad (91)$$

city of the wave; here, each branch consists of one D bears no resemblance with approximation (90)

except that c can be approxi increasing k, there is a tenc with the "main branches" (the corresponding modes b need further investigation.

The last model run to b gravity waves and illustrate short waves. A set of white- in the range $15 \leq k < 40$ wave with the amplitude A $\tau = 1000$ with $\Delta\tau = 0.01$.

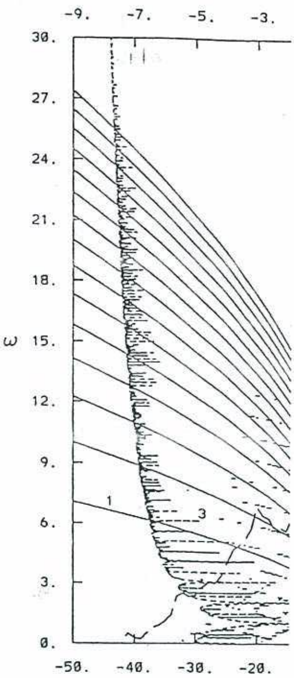

Figure 20: Same spectral chara linear dispersion relation $\omega^2 = k$ the Stokes wave ($\omega = ck$).

except that c can be approximated by the linear phase velocity (59). With increasing k, there is a tendency for the branches to straighten. Along with the "main branches" (89), there are other patterns in the spectra; the corresponding modes bear relatively low energy. These structures need further investigation.

The last model run to be described (Exp. 10) again deals with pure gravity waves and illustrates interaction of a large long wave with small short waves. A set of white-noise-like waves with the amplitude of 0.001 in the range $15 \le k < 40$ was superimposed on a 2π-periodic Stokes wave with the amplitude $A = 0.3$. The integration was performed up to $\tau = 1000$ with $\Delta\tau = 0.01$.

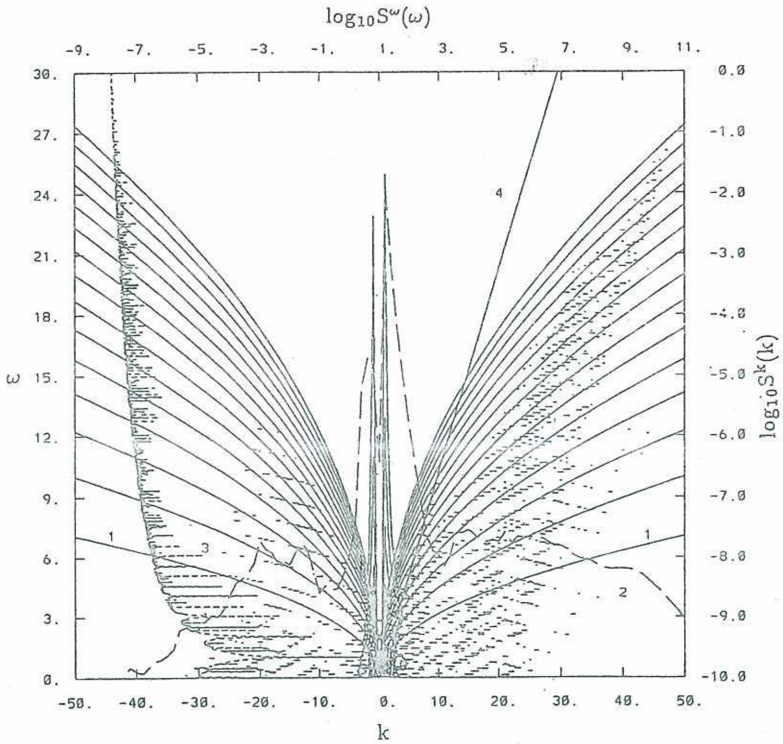

Figure 20: Same spectral characteristics as in Fig. 8 but for Exp. 10. Curve 1 – linear dispersion relation $\omega^2 = k$, 2 – $\log_{10} S^k(k)$; 3 – $\log_{10} S^\omega(\omega)$, 4 – components of the Stokes wave ($\omega = ck$).

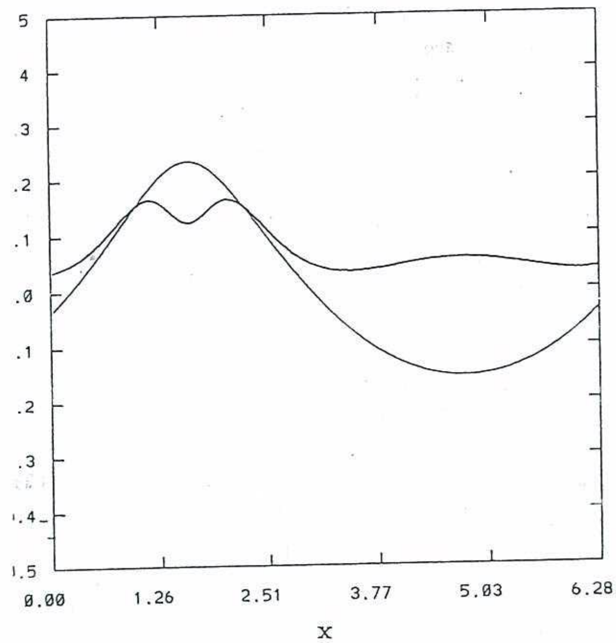

Distribution of the time-averaged potential energy of perturbations (mul-
100, thick curve) over the phase of the running Stokes-like wave (thin curve,
by time averaging of the surface profile) (Exp. 10). The averaging is per-
a coordinate system moving with the component $k = 1$.

e evolution of the wavenumber spectrum is given in Fig. 18 which
aat the energy of the main Fourier components of Stokes wave
d virtually unchanged while the energy of the short waves de-
considerably during the integration. The dependence of phase
(77) on wavenumber differs substantially from the correspond-
lts of the previously described runs: it bears little resemblance
e linear-theory dependence (59) (the curve in Fig. 19). Corre-
gly, in the wavenumber–frequency spectra (Fig. 20) the "main
s" (89) appear to be represented only by the Fourier components
tokes wave and so are described by (91), while the superimposed

waves belon
ent from th
was used as
havior of th
with the Sto
that the dis
phase of the
shows clear

7. Concl

The behavio
Even for the
isolated case
ary pure gr
for consecut
truncated F
which the a
cation numb
investigatio
may lead to
ical algorith
made durin
for simulatio
been proven
develop a hi
potential wa
of wave phe
theoretical

The ma
tionary pot
a numerical
be eliminat
surface-follo
most effecti
of long-term

The res

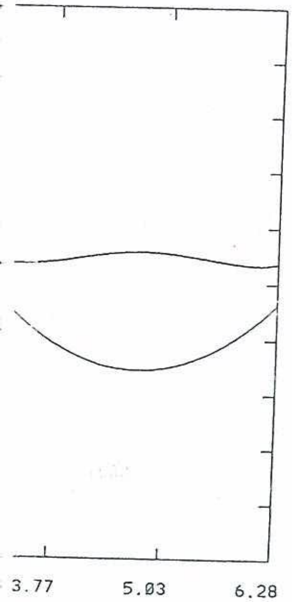

potential energy of perturbations (mul-
the running Stokes-like wave (thin curve,
ofile) (Exp. 10). The averaging is per-
the component $k = 1$.

spectrum is given in Fig. 18 which
urier components of Stokes wave
he energy of the short waves de-
ration. The dependence of phase
ibstantially from the correspond-
runs: it bears little resemblance
) (the curve in Fig. 19). Corre-
ncy spectra (Fig. 20) the "main
d only by the Fourier components
l by (91), while the superimposed

waves belong to additional regular patterns which are completely different from those observed in Exp. 6 (Fig. 11) where "pure" white noise was used as the initial conditions. The difference suggests that the behavior of the superimposed waves is strongly controlled by interactions with the Stokes wave. The same conclusion can be drawn from the fact that the distribution of the energy density of the short waves over the phase of the Stokes wave (Fig. 21) is far from uniform or chaotic, and shows clear maxima at the points of maximum slope of the Stokes wave.

7. Conclusions

The behavior of nonlinear waves is difficult to investigate analytically. Even for the stationary equations, exact solutions are known only in the isolated case of pure capillary (Crapper's) waves. In the case of stationary pure gravity (Stokes) waves, construction of analytical expansions for consecutive Fourier coefficients provides only an approximation for truncated Fourier series and is thus, actually, a numerical procedure in which the amount of calculations increases sharply with increasing truncation number. As for general nonstationary wave fields, their analytical investigation is clearly impossible without drastic simplifications which may lead to unpredictable consequences. In the development of numerical algorithms for 1-D potential waves, considerable progress has been made during the last 15 years, but the applicability of these techniques for simulation of multi-mode wave fields over a long time period has not been proven. One possible approach to circumvent these problems is to develop a highly accurate numerical scheme for the principal equations of potential waves. With such a scheme, direct hydrodynamical modeling of wave phenomena may be expected to provide improvements in many theoretical and applied aspects of wave studies.

The main difficulty in constructing numerical methods for nonstationary potential waves is how to deal with the vertical dimension. For a numerical scheme to be really efficient, the vertical dimension must be eliminated from the model prognostic equations. The nonstationary surface-following conformal mapping used in our scheme is, indeed, a most effective way to resolve this problem and make the model capable of long-term multi-mode simulations.

The results obtained in this work may be divided into three groups.

al mapping developed by Stokes (1848) for sta-
as extended to the nonstationary case, where
ion becomes time dependent, and the surface-
o longer the velocity potential and the stream
ved effective because the original system con-
on and two nonlinear boundary conditions on
duced, without any simplification, to a system
nstationary equations. As in the Cartesian
t variables are the elevation and the velocity
t their dependence on the Cartesian horizontal
l parametrically via the new horizontal coordi-
ystem may be solved by numerical integration,
y calculating nonlinearities via Fourier trans-
may also be used for analytical investigations
developed for the original system, with the
the problem of extrapolating the velocity po-
not exist.

solution of the stationary equations for gravity
s has been developed. The method allows us to
omputer accuracy and is based on representa-
ation for the surface height, written in the new
case are proportional to the velocity potential
via operators of integration and (generalized)
lculated in Fourier space. Again, the use of
to calculate nonlinearities allows a highly ef-
the method. It should be noted that we had
gorithms for pure gravity and gravity-capillary
ter case our algorithm fails to converge when
arity coefficient becomes small. This problem
igations. It was shown that, with decreasing
cient, the phase velocities of gravity-capillary
n approach the values of the Stokes phase ve-
aves do not appear to be an asymptotic form of
as the capillarity goes to zero. This, together
e algorithm (and its various modifications) for
an indication that stationary gravity-capillary
tly affected by capillary forces are unstable or

While properties of statio
lems, we used these results m
model. The validation was pe
tion 3 as initial conditions for
dinate system of the latter wa
wave profile, the model simu
waves. It should be emphasiz
as the nonstationary model is
than the stationary ones and
"does not know" that the sin
shape. Nevertheless, they di
amplitudes. This suggests th
are stable with respect to tru
and (2) these errors are small

3. We used the nonstationary
linear wave fields. The cases d
arbitrarily, as our aim was to
plications of the technique de
most clearly seen in the simu
ratory experiment by Yuen a
of multi-mode wave fields wa
frequency spectra into regula
energy concentrated along wh
branches satisfies a dispersion
the number n of the branch is
and is greater than 1 for branc
In this structure, nonlinear eff
of multiple branches and in de
the linear dispersion relation f
cases the deviation clearly appe
a straight line and so the grou
this effect needs further analy
duced other regular branches.
these additional branches was
remarkable exception of a pecu
at least for not too small wave
by a straight line passing thro
was perhaps most strongly ma

While properties of stationary solutions imply many intriguing problems, we used these results mainly as a tool to validate the nonstationary model. The validation was performed by using solutions obtained in Section 3 as initial conditions for the nonstationary problem. Since the coordinate system of the latter was bound to the mean flow rather than to the wave profile, the model simulates running Stokes and gravity-capillary waves. It should be emphasized that the validation was far from trivial, as the nonstationary model is based on equations much more complicated than the stationary ones and on a numerical procedure of its own, which "does not know" that the simulated waves are supposed to retain their shape. Nevertheless, they did retain it surprisingly well even for large amplitudes. This suggests that (1) Stokes and gravity-capillary waves are stable with respect to truncation errors of the nonstationary model, and (2) these errors are small.

3. We used the nonstationary model for case studies of evolution of nonlinear wave fields. The cases described in Section 6 were chosen somewhat arbitrarily, as our aim was to provide a possibly broader variety of applications of the technique developed. The effects of bound waves were most clearly seen in the simulation designed to approximate the laboratory experiment by Yuen and Lake (1982). A most surpising feature of multi-mode wave fields was a clear separation of the wavenumber–frequency spectra into regular curvilinear branches, with most of the energy concentrated along what we called "main branches". This set of branches satisfies a dispersion relation whose form is given by (89) where the number n of the branch is 1 for the branch consisting of free waves and is greater than 1 for branches consisting of generalized bound waves. In this structure, nonlinear effects were manifested both in the existence of multiple branches and in deviation of the "parent" curve ($n = 1$) from the linear dispersion relation for relatively large wavenumbers. In most cases the deviation clearly appeared to be such that the curve approaches a straight line and so the group velocity tends to a constant; however, this effect needs further analysis. The nonlinear interactions also produced other regular branches. The energy of the modes belonging to these additional branches was usually very small, sometimes with the remarkable exception of a peculiar pattern (or group of patterns) which, at least for not too small wavenumbers, could be roughly approximated by a straight line passing through the origin. The nonlinear behavior was perhaps most strongly manifested in the case of a long Stokes wave

t waves, where the free wave branch is ;ation of short waves is largely controlled wave. On the other hand, the nonlinear ıbers was remarkably larger in the case ι in all other runs, which included pure es simulations with the same initial sur- s further investigation, as the structure of ːrtum was partially obscured by apparent

ːe may be used to study a variety of prob- amics:

ıear wave fields in a wide range of wavenum- fficients;

d long waves;

ve models by use of the developed hydro- ː of moving wave surfaces;

ıich can be studied by coupling of the de- ndary layer model (e. g. Chalikov, 1978,

. V. Zakharov for helpful discussions and ransform to resolve the model equations ives; Dr D. B. Rao, Dr W. Perrie, and Dr uscript and making many valuable com-

nulation of wind-wave interaction. *Jour-* 1 – 582.

simulation of the boundary layer above

waves. *Bound Layer Met*, 1986, 3

3. Chalikov, D.V. & Liberman Yu for potential waves. *Izv. Sov. Atn*

4. Craig, W. & Sulem, C. Numeri *nal of Comp Phys*, 1993, **108**, 73 -

5. Crapper, G.D. An exact soluti arbitrary amplitude. *Journal of Fl*

6. Crapper, G.D. Introduction to \ 1984, 224 pp.

7. Dold, J.W. An Efficient Surfac steady Gravity Waves. *Journal of* (

8. Donelan, M.A. & Hui, W.H. Me *face Waves and Fluxes* eds Geerna demic, Dordrecht, 1990, vol. 1, 209

9. Drennan, W.M., Hui, W.N. Ten water waves of large amplitude. *Z.* 380.

10. Eliassen, E.B., Machenhauer, I method for integration of the hydro representation of the horiszontal fiel Meteorologi, Københavens Universi

11. Hasselmann, K. On the nonline spectrum, part 1: General theory. *J* – 500.

12. Kuznetsov, E.A., Spector, M.D. gularities on the free surface of an ic No. 2, 1283 – 1290.

13. Lake, B.M. & Yuen, H.C. A ne

where the free wave branch is
short waves is largely controlled
n the other hand, the nonlinear
s remarkably larger in the case
ther runs, which included pure
tions with the same initial sur-
investigation, as the structure of
s partially obscured by apparent

used to study a variety of prob-

fields in a wide range of wavenum-

aves;

s by use of the developed hydro-
ng wave surfaces;

be studied by coupling of the de-
ver model (e. g. Chalikov, 1978,

narov for helpful discussions and
to resolve the model equations
D. B. Rao, Dr W. Perrie, and Dr
nd making many valuable com-

of wind-wave interaction. *Jour-*

n of the boundary layer above

waves. *Bound Layer Met*, 1986, 34, 63 – 98.

3. Chalikov, D.V. & Liberman Yu.M. Integration of primitive equations for potential waves. *Izv. Sov. Atm. Ocean Phys.*, 1991, 27, 42 – 47.

4. Craig, W. & Sulem, C. Numerical Simulation of Gavity Waves. *Journal of Comp Phys*, 1993, 108, 73 – 83.

5. Crapper, G.D. An exact solution for progressive capillary waves of arbitrary amplitude. *Journal of Fluid Mech*, 1957, 96 ,417 – 445.

6. Crapper, G.D. Introduction to Water Waves, John Wiley, Chichester, 1984, 224 pp.

7. Dold, J.W. An Efficient Surface-Integral Algorithm Applied to Unsteady Gravity Waves. *Journal of Comp Phys*, 1992, 103 90 – 115.

8. Donelan, M.A. & Hui, W.H. Mechanics of ocean surface waves. *Surface Waves and Fluxes* eds Geernaert, G.L., Plant, W.J., Kluwer Academic, Dordrecht, 1990, vol. 1, 209 – 246.

9. Drennan, W.M., Hui, W.N. Tenti G. Accurate calculatioms of Stokes water waves of large amplitude. *Z. angew Math Phys*, 1992, 43, 367 – 380.

10. Eliassen, E.B., Machenhauer, B. & Rasmussen, E. On a numerical method for integration of the hydro-dynamical equations with a spectral representation of the horiszontal fields. Report 2, Institute for Teoretisk. Meteorologi, Københavens Universitet, Copenhagen, Denmark, 1970.

11. Hasselmann, K. On the nonlinear energy transfer in a gravity-wave spectrum, part 1: General theory. *Journal of Fluid Mech*, 1962, 12, 481 – 500.

12. Kuznetsov, E.A., Spector, M.D. & Zakharov, V.E. Formation of singularities on the free surface of an ideal fluid. *Physical review*, 1994, 49, No. 2, 1283 – 1290.

13. Lake, B.M. & Yuen, H.C. A new model for nonlinear wind waves.

al model and experimental evidence. *Journal of Fluid* 33 – 62.

gins, M.S. Integral properties of periodic gravity waves le. *Proc. R. Soc. Lond.*, 1975, A **342**, 157 – 174.

;gins, M.S. & Cokelet, E.D. The deformation of steep water. I. A numerical method of computation *Proc. R.* , **350**, 1 – 26.

. Transform method for calculation of vector coupled n to the spectral form of vorticity equation, *Journal of* **27**, 890 – 895.

A. & Jacobs, J.W. A Numerical Method for Potential Surface. *Journal of Comp Phys*, 1983, **51**, 365 – 386.

On the theory of oscillatory waves. *Trans. Cambridge* :41-445. *Math. Phys. Pap.*, 1847, **1**, 197 – 229.

1880 Supplement to a paper on the theory of oscillatory *ys. Pap.*, 1880, **1**, 314 – 326.

. & West B.J. A transport-equation description of non- ,ce wave interactions. *Journal of Fluid Mech*, 1975, **70**,

rueckner K.A. & Janda R.S. A New Numerical Method ɔdynamics. *Journal of Geophys. Res.*, 1987, **92**, No. ;24.

Lake B.M. Nonlinear Dynamics of Deep-Water Gravity *pl Mech*, 1982, **22**, 67 – 229.